Subsurface Radar Sounding of the Jovian Moon Ganymede

This paper gives an overview of the radar designed to orbit Jupiter and investigate Jupiter's icy moons, which are suspected of hiding a liquid ocean below their thick ice shell.

By Lorenzo Bruzzone, *Fellow IEEE*, Giovanni Alberti, Claudio Catallo, Adamo Ferro, *Student Member IEEE*, Wlodek Kofman, and Roberto Orosei

ABSTRACT | This paper provides an overview of the Europa Jupiter System Mission (EJSM) and of its scientific objectives, focusing the attention on the subsurface radar (SSR) instrument included in the model payload of the Jupiter Ganymede Orbiter (JGO). The SSR instrument is a radar sounder system at low frequency (HF/VHF band) designed to penetrate the surface of Ganymede icy moon of Jupiter for performing a subsurface analysis with a relatively high range resolution. This active instrument is aimed at acquiring information on the Ganymede (and partially on the Callisto during flybys) shallow subsurface. The paper addresses the main issues related to SSR, presenting its scientific goals, describing the concept and the design procedure of the instrument, and illustrating the signal processing techniques. Despite the fact that SSR can be defined on the basis of the heritage of the Mars Advanced Radar for Subsurface and Ionosphere Sounding (MARSIS) and SHAllow RADar (SHARAD) instruments currently operating at Mars, the EJSM mission poses additional scientific and technical challenges for its design: 1) the presence of a relevant Jupiter radio emission (which is very critical because it has a significant power spectral density in proximity of the expected SSR central frequency); 2) the properties of the subsurface targets, which are different from those of the Mars subsurface; 3) the different orbit conditions; and 4) the limited available resources (in terms of mass, power, and downlink data rate). These challenges are analyzed and discussed in relation to the design of the instrument in terms of: 1) choice of the central frequency and the bandwidth; 2) signal-to-noise ratio (SNR); 3) signal-to-clutter ratio (SCR); and 4) definition of the synthetic aperture processing. Finally, the procedure defined for SSR performance assessment is described and illustrated with some numerical examples.

KEYWORDS | Callisto; Europa; Europa Jupiter System Mission; Ganymede; ground penetrating radar; Jupiter; radar sounding; subsurface radar

I. INTRODUCTION

The Europa Jupiter System Mission (EJSM) is one of the major joint European Space Agency (ESA) and National Aeronautics and Space Administration (NASA) missions in the Solar System currently under study [1]. It is aimed at exploring Jupiter and its icy moons with payloads based on advanced concepts. The architecture of the mission is based on two spacecrafts having different complementary goals: the Jupiter Europa Orbiter (JEO), provided by NASA and devoted mainly to study Jupiter and the Jovian moons Io and Europa, and the Jupiter Ganymede Orbiter (JGO), which represents the contribution of ESA and will investigate Jupiter and the Ganymede and Callisto moons. The two spacecrafts will be launched independently in early 2020 and their trip to the Jovian system will last approximately six years. In the first science phase, the platforms will tour through the Jupiter system, including many flybys of its moons. In a second phase, JEO and JGO will be inserted in circular orbit around Europa and Ganymede, respectively.

L. Bruzzone and **A. Ferro** are with the Department of Information Engineering and Computer Science, University of Trento, I-38123 Trento, Italy (e-mail: lorenzo.bruzzone@ing.unitn.it; adamo.ferro@disi.unitn.it).
G. Alberti is with the Consorzio di Ricerca su Sistemi di Telesensori Avanzati (CORISTA), I-80125 Naples, Italy (e-mail: alberti@unina.it).
C. Catallo is with Thales Alenia Space Italia, I-00131 Rome, Italy (e-mail: Claudio.Catallo@thalesaleniaspace.com).
W. Kofman is with the Laboratoire de Planetologie de Grenoble CNRS/UJF, F-38041 Grenoble Cedex 9, France (e-mail: wlodek.kofman@obs.ujf-grenoble.fr).
R. Orosei is with the Istituto Nazionale di Astrofisica, Istituto di Fisica dello Spazio Interplanetario, I-00133 Rome, Italy (e-mail: roberto.orosei@ifsi-roma.inaf.it).

The overarching theme of the EJSM mission is the study of the emergence of habitable worlds around the gas giant Jupiter. In this context, the scientific return of the mission will be substantially increased by the synergistic analysis of the measurements made by each single platform. To this end, the science payloads of the two spacecraft include instruments peculiar to each platform and instruments with similar properties on both spacecraft for correlating measures carried out on different moons.

In agreement with the mission concept, the core payloads of both platforms include a radar sounder instrument. Radar sounders are active instruments (similar in concept to terrestrial ground penetrating radars) that are based on the transmission of radar pulses at frequencies in the midfrequency (MF), high-frequency (HF), or very high-frequency (VHF) portions of the radio spectrum into the surface and the subsurface. The detected echoes (associated with reflected signals) from both the surface topography and the subsurface structures (e.g., see [2]) are processed in order to construct radargrams that contain detailed information on the subsurface structure, pointing out the interfaces between different layers. Radar sounders are effective on ice as it is the most transparent natural material in the aforementioned range of frequencies. This is particularly true for Jupiter's icy moons, as the cold temperature of the ice in the outer Solar System increases the propagation capabilities with respect to the case of warm ice [3].

In the current phase of design of the mission, the radar sounders included in the EJSM payloads are called subsurface radar (SSR) for JGO and ice penetrating radar (IPR) for JEO. SSR is defined as a single-frequency radar sounder aimed at investigating the shallow subsurface of Ganymede (mainly during the circular orbit phase) and in a more limited way of Callisto (during some flybys) in a depth range of few kilometers (< 5 km) with high vertical resolution (< 15 m) [4]. IPR is a dual-frequency system that can also work in a deep investigation mode in order to characterize the subsurface of Europa up to a depth of 30 km with a lower vertical resolution (< 100 m), besides a shallow investigation mode similar to the SSR single mode [1]. The measurements possible with these instruments will provide important and unique information about the evolution of the Jovian moons and their subsurface and near-surface structures, as well as contribute to answer to the question about the existence of an internal subsurface ocean on Europa.

SSR and IPR have some similar basic properties. Both exploit the common heritage from the radar sounders developed for two recent Mars missions: Mars Advanced Radar for Subsurface and Ionosphere Sounding (MARSIS) on ESA's MARS Express [5], and Mars SHAllow RADar (SHARAD) on NASA's Mars Reconnaissance Orbiter [6].

This paper focuses on the SSR instrument for JGO discussing the most important concepts and the technological challenges related to the development of this system. As mentioned before, the main target of SSR is Ganymede, which will be deeply investigated during the last part of the JGO mission when the spacecraft will be inserted in circular orbit around this moon. This phase is expected to take 180 days. However, before the Ganymede orbit insertion, JGO will perform also a number of flybys of Callisto [1]. Therefore, SSR will be able to partially investigate also the subsurface of Callisto.

Although the EJSM mission is currently under study and the requirements and properties of the SSR instrument are still under investigation and cannot be analyzed in detail at this point of the development phase, there are some important and challenging issues that have been preliminary identified and are peculiar for the design of SSR with respect to previous radar sounding instruments used for the exploration of Mars. The paper addresses these key issues, providing a general view of the scientific goals of SSR and discussing the major challenges related to the Jovian environment that affect the definition of the instrument. The latter are the Jovian radio emission, which can strongly affect the instrument measurements, and the properties of the surface and subsurface targets that will be measured by the radar. In addition, the main technical design issues are discussed in terms of: 1) choice of the central frequency and the bandwidth for obtaining the required tradeoff between penetration capability and range resolution; 2) signal-to-noise ratio (SNR); 3) signal-to-clutter ratio (SCR); and 4) definition of the synthetic aperture processing. Moreover, the procedure defined for SSR performance assessment is described and illustrated with some numerical examples.

The paper is organized into six sections. Section II presents the main scientific goals related to the SSR instrument on JGO. Section III illustrates the instrument concept and reports its general description. Section IV proposes an analysis of the major scientific and technical challenges related to the Jovian environment that are associated with the definition of SSR, while Section V illustrates the main design issues of the instrument. Section VI presents the procedure defined for SSR performance assessment. Finally, Section VII draws the conclusion of this paper.

II. SCIENTIFIC GOALS OF SSR

Ganymede and Callisto are the third and the fourth of the so-called Galilean moons, respectively, the first two in order of distance being Io and Europa (see Fig. 1). Their orbits around Jupiter have semimajor axis of 421 800 km (Io), 671 100 km (Europa), 1 070 400 km (Ganymede), and 1 882 700 km (Callisto).

In the current mission architecture, the JGO spacecraft is expected to perform several flybys at Ganymede and Callisto before entering in circular orbit around Ganymede. Despite the fact that the SSR instrument
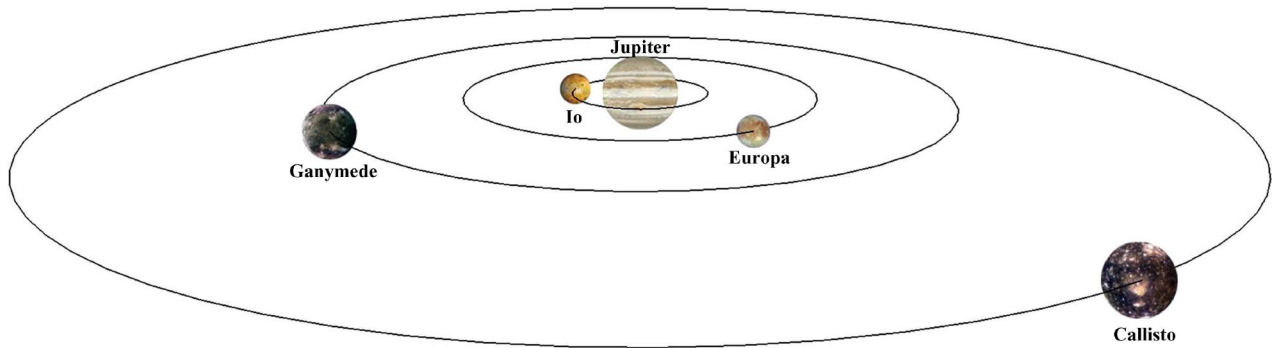
Fig. 1. *Three-dimensional view of the Galilean moons of Jupiter. The orbit radii and the moon sizes are in scale. Jupiter size is not in scale.*

should operate during all these flybys, acquiring data at both Ganymede and Callisto [1], the circular phase around Ganymede will be the main target for radar observations. Thus, the scientific objectives for the experiment have been defined by the mission science definition team with a special focus on Ganymede. These objectives, can be summarized as follows [4].

- *Identification of the stratigraphic and structural patterns of Ganymede*: 1) reconstruction of the stratigraphic geometries of the ice strata and bodies and their internal relations, definition of the unconformities and identification of the formation processes; 2) recognition, analysis, and mapping of the tectonic features; 3) inference and analysis of the material present in the subsurface and their metamorphism linked to the burial process.

- *Crustal behavior*: 1) analysis of the stratigraphic and structural data to identify the mode of accretion of the crust and its consumption matched by the deformational processes; 2) estimation of the ice deposition rate; 3) identification of evidences for degassing of the Ganymede's interior.

- *Matching the surface geology with subsurface features*: joint analysis of the surface and subsurface geology in order to understand the depositional and tectonic processes active in the uppermost icy crust and to infer the subsurface nature in areas without radar data.

- *Global tectonic setting and Ganymede's geological evolution*: 1) understanding the large-scale geological processes active in the Ganymede at the global scale; 2) global mapping of the different geological realms based on the surface and subsurface geology; 3) reconstruction of the geological evolution of Ganymede.

- *Comparison between Ganymede and Europa*: definition of the differences and common geological patterns of the two planetary bodies for a better understanding of the development of the icy

moons and the geological principles at the basis of the icy bodies evolution.

- *Altimetry on Ganymede*.

The aforementioned scientific goals can be related also to Callisto (when applicable). However, they should be properly downscaled due to the availability of only a few short and fast flybys along an elliptical orbit (i.e., without entering into orbit around the moon).

These objectives require that the radar can characterize with adequate horizontal and vertical resolutions the dielectric, thermal and mechanical discontinuities resulting from the geologic processes that shape the crust of the two moons. The main performance requirements are described in [4], and are as follows:

- penetration depth: up to 5 km;
- along-track resolution: < 1 km;
- across-track resolution: < 5 km;
- vertical resolution: 15 m (in free space).

III. SUBSURFACE RADAR INSTRUMENT

The SSR instrument is an active radar sounder with a nadir-looking geometry designed to acquire subsurface echo profiles of the investigated icy moons (see Fig. 2). The theoretical basis of this instrument is related to radio-echo sounding (or ice penetrating radar), which is a well-established geophysical technique that has been used for more than four decades to investigate the internal structure of the ice sheets and glaciers on the Earth at Antarctica, in Greenland, and in the Arctic [2]. Radar sounders transmit toward the surface a radar pulse at a frequency selected in the MF, HF, or VHF portion of the electromagnetic spectrum. Thanks to the relatively low frequency and the nadir-looking geometry, only a portion of the transmitted pulse is backscattered from the surface, while a significant part of the pulse is propagated to the subsurface icy layers. The coherent echoes backscattered from the subsurface interfaces within each resolution cell (defined by the along-track and across-track resolutions) are detected by the receiver and visualized in the resulting
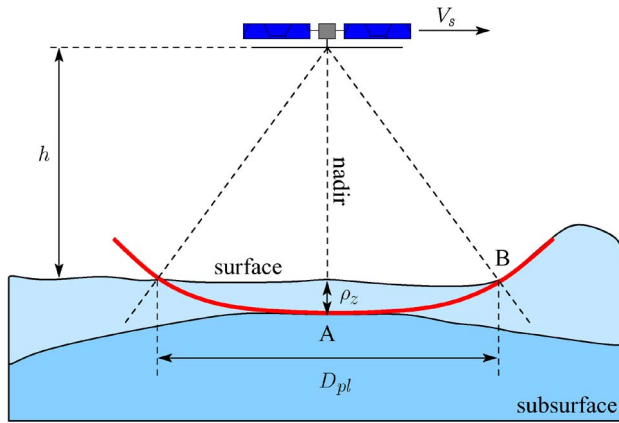
Fig. 2. *Geometry of a nadir-looking radar sounder: h is the altitude of the spacecraft orbit; V_s indicates the spacecraft speed; ρ_z depicts the system range resolution; and D_{pl} is the pulse-limited resolution cell. If the topography is not flat, during pulse transmission off-nadir areas (B) are reached by the signal wavefront at the same time as subsurface reflections from nadir (A). Therefore, during reception lateral echoes reach the antenna at the same time as nadir echoes, generating the so-called clutter problem. The vertical dimension of the figure is not in scale* ($h \gg \rho_z$)*.*

Fig. 4. *Interfaces of the subsurface radar instrument.*

radargram. The backscattering from the subsurface is driven by different dielectric, related to mechanical, thermal, or compositional discontinuities that the radiation intercept along its path.

A block diagram of the SSR architecture is presented in Fig. 3. The instrument is made up of a deployable dipole antenna and three main subsystems: the transmit front-end (TFE) subsystem, the receiving subsystem (RX), and the digital electronics subsystem (DES). The DES envelopes the command and control functions (Ctrl) interfacing with the spacecraft bus, the processing capabilities to pre-elaborate the science data collected during the observations (Signal proc.), as well as the digital synthesis of the radar pulse (Digital Chirp Gen.) and the generation of all needed system timings and frequencies (Timing & Freq.). The frequency-modulated radar pulses (chirp) are digitally generated directly at the transmit frequency so that no conversion is needed. The signal is amplified (Power
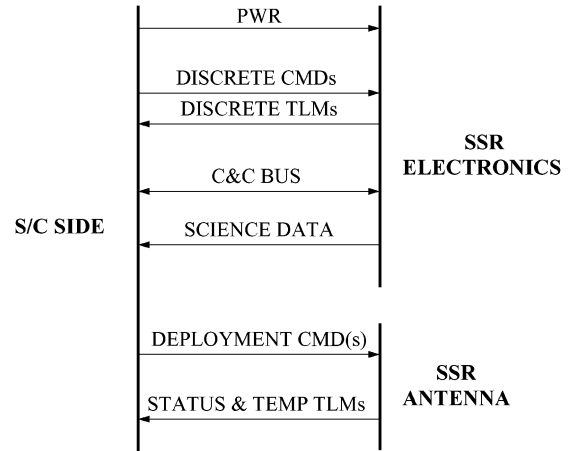
Amp.) at the required power level and then sent to the antenna matching network (Matching) within the TFE. The RX is based on a direct conversion approach with downsampling. The received signal is amplified by a low noise amplifier (LNA), filtered and routed to the analog-to-digital converter (ADC) by adjusting its amplitude by means of an automatic gain control device (AGC).

Fig. 4 shows the expected interfaces between the SSR subsystems and the JGO spacecraft, which are as follows.
- Spacecraft (S/C) from/to radar DES subsystem:
  - power (PWR) voltage;
  - discrete commands (CMDs) such as radar on–off and AGC;
  - discrete telemetry (TLMs) containing voltage and current values, and temperature values provided by onboard thermistors;
  - controls and command signals (C&C BUS) such as Tx/Rx gate, ADC start/stop, digital chirp generation start/stop;
  - science data consisting in the digitalized received echoes.
- Spacecraft from/to radar antenna subsystem:
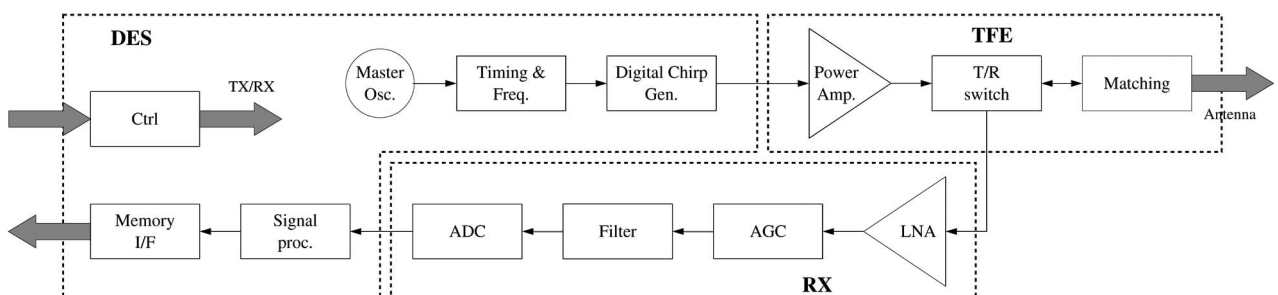 - signals for deployment;

Fig. 3. *Architecture of the subsurface radar instrument.*

- telemetry data (STATUS & TEMP. TLMs) containing antenna status and temperature values provided by onboard thermistors.

IV. TECHNICAL CHALLENGES RELATED TO THE JUPITER/GANYMEDE ENVIRONMENT

This section describes the most important challenges for the definition of the SSR instrument in the Jovian system environment. Here we focus on two fundamental issues: 1) the electromagnetic radiation noise, and 2) the properties of the surface and subsurface targets that should be investigated by the radar. These two issues considerably affect the design of the instrument and its acquisition strategy.

A. Spectrum of the Jupiter Radio Emission

Jupiter is a bright radio object. As seen from Earth, Jupiter's radio brightness is exceeded only by the Sun's. The radio spectrum of the planet in the range from kilohertz to gigahertz is dominated by nonthermal radiation generated in the inner magnetosphere. In the frequency range above 100 MHz, emission is continuous and dominated by synchrotron radiation. The most intense radio emission occurs in the frequency range between few megahertz and about 40 MHz [7], and it is expected to be due to cyclotron radiation originating in and above the ionosphere on magnetic field lines that thread the Io plasma torus [7]. In this range of frequencies, emission is highly variable in space and time, but shows a strong correlation with the position of the observer, due to beaming effects [8] and to the Io's moon phase [9]. Lesser enhancements of emission intensity correlate with the orbital phase of Ganymede [10], Callisto [11], and Europa [12], most likely as a result of Alfvén currents along magnetic field lines near moons' orbits. It was found that Jupiter radio emission is influenced also by solar wind [13].

The full radio spectrum of Jupiter has been determined by the Planetary Radio Astronomy (PRA) experiment on both Voyager spacecrafts and by the Cassini Radio and Plasma Wave Science instrument (RPWS). It can be seen in Fig. 5 that the peak flux densities can be up to 100 times the average values. It is thus evident that the Jupiter radio spectrum is critical and should be properly considered in the phase of selection of the radar sounder carrier frequency.

B. Properties and Models of the Surface and Subsurface Targets

Ganymede is the largest moon of the Solar System, larger than Mercury, and is also the only moon having an intrinsic magnetic field [17]. The main geologic classification of the surface is between dark and bright terrains [18]–[20]. Dark terrain covers about one third of the surface and is heavily cratered, suggesting a very ancient, if
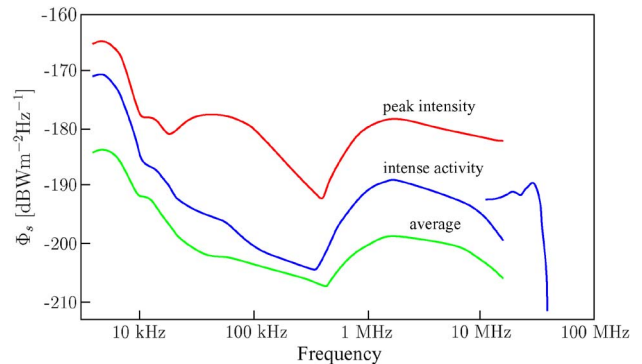
Fig. 5. *Jupiter radio spectrum based on Cassini-RPWS data [14], normalized to a distance of 1 AU. Green curve: rotation averaged emission. Blue curve: rotation averaged emission at times of intense activity. Red curve: peak intensities during active periods. Due to the Earth's ionosphere, frequencies below ~5–10 MHz are not accessible to ground-based observations, so the full radio spectrum of Jupiter could only be determined by the PRA experiment on both Voyager spacecrafts [15]. Recently, the spectrum was recalculated with much more accuracy using Cassini RPWS data [14]. The figure is taken from [8] and is based on that spectrum. Unfortunately, Cassini-RPWS data are only available for frequencies $f \leq 16$ MHz. For higher frequencies, spectral data from [16] are shown, which correspond to periods of intense emission activity [14].*

not primordial, origin. Bright terrain separates dark terrain into polygons, and contains both smooth bright surfaces and materials with closely spaced parallel ridges and troughs (termed grooved) that are dominated by extensional tectonic features [21], [22]. Ganymede's surface is composed mostly of water ice [19], although its relatively low albedo is determined by the presence of darker non-ice materials, which may be hydrated frozen brines similar to those inferred for Europa [23]. An image of the Ganymede's surface including examples of both bright and dark terrains is shown in Fig. 6.

The possible internal structures of Ganymede and Callisto are shown in Fig. 7. The interior of Ganymede has been modeled from gravity data, and appears to be differentiated into an outermost ~800-km-thick ice layer and an underlying silicate mantle. A central iron core might also be present, which would explain the existence of a magnetic field. Ganymede has internal mass anomalies, perhaps related to topography on the ice-rock interface [24], [25]. Results from the magnetometer onboard the Galileo probe may indicate the presence of an internal ocean within 100–200 km of Ganymede's surface, but inference is less robust than at Europa and Callisto [26]. The Ganymede surface is more cratered and ancient than Europa's, consistent with a much thicker outer shell of solid ice. The role of icy volcanism in modifying the surfaces of outer planet moons is an outstanding question about which little is truly understood. Like many other icy moons, there is ambiguous evidence for cryovolcanic processes modifying the surface of Ganymede.
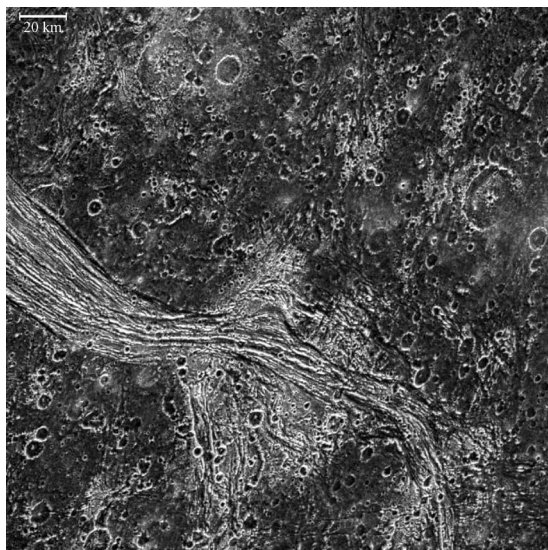
Fig. 6. *Image PIA01617 taken from NASA's Photojournal web site (http://photojournal.jpl.nasa.gov) showing a highly fractured lane of bright light grooved terrain (Lagash Sulcus) which runs through an area of heavily cratered dark terrain within Marius Regio on Jupiter's moon Ganymede. The boundary between these two units is marked by a deep trough. North is to the top of the picture and the sun illuminates the surface from the upper right. The image, centered at 17° South latitude and 156° longitude, covers an area of approximately 230 × 230 km². (Image Credit: NASA/JPL/Brown University.)*

Callisto is supposed to be composed of approximately equal amounts of rock and ice, which make it the least dense of the Galilean moons. Investigation by the Galileo spacecraft revealed that Callisto may have a small silicate core and possibly a subsurface ocean of liquid water at depths greater than 100 km [27]. The surface of Callisto is heavily cratered and extremely old (it is one of the most heavily cratered in the Solar System). It does not show any signature of subsurface processes such as plate tectonics or volcanism, and is thought to have evolved predominantly under the influence of impacts [28].

Although any subsurface ocean of Ganymede is almost certainly too deep to be detected by the radar (see estimates of ice crust thickness in [29]), all geologic processes shaping and reworking the crust of the moon are expected to have produced stratifications that could reflect electromagnetic waves due to dielectric, mechanical, or thermal discontinuities. Dielectric discontinuities are changes in the content of impurities in water ice due to deposition of material from meteoric impacts or cryovolcanic processes. Mechanical discontinuities are produced by tectonic processes, such as faulting. As the dielectric properties of water ice depend significantly on temperature, subsurface cryovolcanic magma or the transition between a conductive and a convective layer in the crust would also produce a radar reflection.

The crust of Ganymede should be predominantly composed of water ice down to depth of a few hundreds of kilometers. At the pressures (from zero to several megapascals) and temperatures expected in the first few kilometers of the icy crust (between 100 and 150 K; see, e.g., [29]), ice is in phase Ih, the hexagonal crystalline ice commonly found on the Earth. The relative dielectric permittivity of water ice in the HF and VHF frequencies (i.e., in the range where the operative frequency of the radar will be selected) is constant, and is close to 3.17 ± 0.7 for temperatures below $-10\,^{\circ}\text{C}$. The measurements
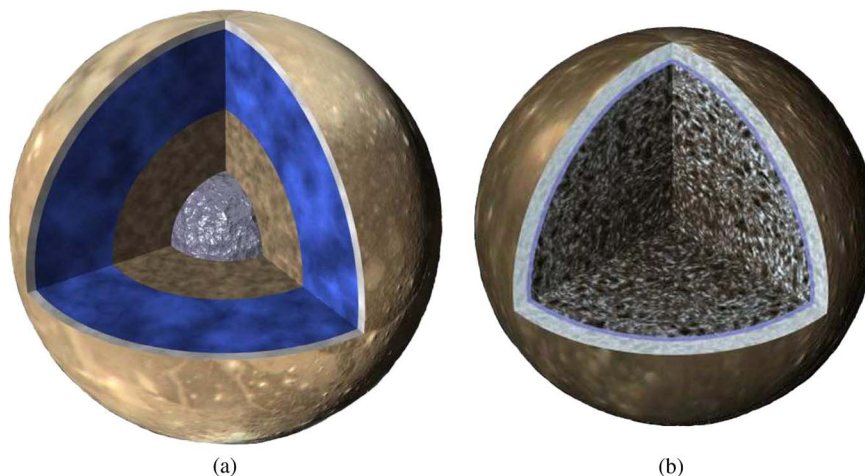
Fig. 7. *Details of image PIA01082 taken from NASAs Photojournal web site (http://photojournal.jpl.nasa.gov) showing cutaway views of the possible internal structures of the Galilean moons Ganymede (a) and Callisto (b). Ganymede's radius is 2634 km, while Callisto's is slightly smaller at 2403 km. Ganymede has a metallic (iron, nickel) core (shown in gray) surrounded by a rock (shown in brown) shell, in turn surrounded by a shell of water in ice or liquid form (shown in blue and white). All shells are drawn to the correct relative scale. Callisto is shown as a relatively uniform mixture of comparable amounts of ice and rock. (Image Credit: NASA/JPL.)*

Table 1 Radar Absorptions for Various Ice Types and Temperatures. Attenuation α Is for One-Way Propagation in Decibels per Kilometer at 251 K. Columns I, II, and III Are Computed One-Way Attenuations (in Decibels per Kilometer) for Ice Shells With Base Temperatures of 270, 260, and 250 K, Respectively. The Range of Values for Each of These Corresponds to Surface Temperatures of 50 and 100 K. These Values Are Independent of Shell Thickness Since the Temperature Profile Is Stretched to the Ice Thickness. The M Column Represents the Plausibility of the Ice Type for Europa; O Is Least Likely While 3 Is More Likely, Given the Present Understanding of Europa. More Details About the Considered Ice Types Are Reported in [34]. Surface Temperature on Ganymede Is Estimated to be Around 100 K [29], While the Heat Flux Coming From the Interior Does Not Raise the Temperature of Ice by More Than 10–20 K Over a Depth of 5 km [44], [45]. (Table and Caption Are Adapted From [34])

M	Ice type	Impurity content	α	I	II	III
0	Pure ice	nil	4.5	0.7-1.2	0.25-0.45	0.1-0.15
1	Chloride-dominated Europa ice/ocean	3.5 ppt chlorinity ocean	16	2-3.5	1.3-2	0.8-1.4
2	Rock/ice	1% lunar soil	8	2.5-3	2-2.4	1.8-2
3	Rock/ice	10% lunar soil	10	4-4.5	3.5-4	3-3.5
3	Sulfate-dominated Europa ice/ocean	10 ppt chlorinity ocean	37	4.5-8	3-5.5	2-3.5
1	Chloride-dominated Europa ice/ocean	3.5 ppt chlorinity ocean	50	7-12	5-8.5	3.5-6
1	Rock/ice	50% lunar soil	21	15-16.5	14.5-16	14-15.5
2	Depth-dependent Ronne Ice Shelf marine ice	0-400 μM Cl linear rise surface to bottom	varies	17-28	12-20	8.5-14
2	Sulfate-dominated Europa ice/ocean	10 ppt chlorinity ocean	150	18-30.5	12.5-22	9-15.5
2	Ronne Ice Shelf marine ice	400 μM Cl (0.025 ppt salinity) ice	150	18-30.5	12.5-22	9-15.5
0	Baltic Sea ice	ice grown in ~3 ppt sea water	850 (at 270 K)	25-42.5	13-21.5	8-13.5

showed in [30] indicate that the dielectric permittivity is isotropic within at least 0.5%. More recent measurements [31] show that the anisotropy of the real part of dielectric constant can reach more than 1% for a radar frequency range larger than 1 MHz.

As losses in pure water ice are low, it is expected that the major effect on the absorption of radar waves depends on the nature and concentration of impurities in the ice, which is difficult to evaluate due to uncertainties and lack of knowledge of the physical nature of icy moons. For Ganymede, the presence of hydrated salts was suggested [32]. Within these limitations, most studies found in the literature were focused on Europa, and only very little is known for Ganymede. Therefore, at the present phase of the study, we assume for the dielectric properties of Ganymede (and Callisto) the same range as for Europa, for which more data are available. For Europan ice, the most detailed studies are probably those of Chyba *et al.* [33] and Moore [34]. The latter considered three types of water ice, produced by three basic processes occurring on the Earth: meteoric ice formed by atmospheric precipitations, sea ice formed by the freezing of water close to the atmospheric interface, and marine ice forming beneath ice shelves directly from ocean water. This study concluded that similar processes are likely to occur on Europa as well, and that the most probable form of ice is marine ice [34]. The approach followed by Chyba *et al.* [33] consisted in computing the dielectric properties of an ice matrix containing impurities of different types, using a mixing equation [35], [36] to calculate the dielectric constant of the mixture and the properties of lunar materials as a model for the impurities within the Europan ice. This approach requires many assumptions and provides only some estimations of the dielectric constants that can be used in the evaluation of the radar performance.

Whereas Chyba *et al.* [33] assumed that impurities are essentially rock-like materials, in [34] the effect of soluble impurities such as F^-, Cl^-, NH_4^+, SO_4^{2-}, and H^+ ions was studied. Table 1 (adapted from [34]) shows the attenuation for different types of impurities in ice, based on laboratory measurements, ice temperature modeling for Europa, and some scaling from Earth ice measurements. These data are valid for electromagnetic frequencies of a few tens of megahertz. It can be seen from Table 1 that the attenuation for low-frequency radar signals can range from a few to several tens of decibels per kilometers for one-way propagation. The most likely one-way losses for Europa are estimated to be between 1 and 8 dB/km.

Another phenomenon that could affect propagation in the subsurface of Ganymede is scattering of electromagnetic waves by ice/pore interfaces within the crust. Scattering plays a role similar to that of attenuation, depending strongly on the dimension of cavities (voids) in the medium compared to the wavelength. The Mie or Rayleigh approaches [37] can be used to calculate the extinction of the radar signal.

Electromagnetic waves can also be scattered by any roughness of the surface when it is not smooth at the wavelength scale. Part of the incident radiation would then be scattered in directions different from the specular one (see Section V-C). The scattering of radio waves by surface and by volume irregularities is thus an important frequency-dependent factor that should be taken into account to evaluate the penetration of the radar wave, and the ratio of any subsurface echo to surface clutter. These two parameters are essential to predict the radar performance (see Section VI).

As physical parameters controlling scattering are essentially unknown for the Jovian moons, it is rather difficult to predict their effects with accuracy. For example, Eluszkiewicz [38] demonstrated that the presence of any ice regolith about 1 km thick with 1% of cavities whose size is comparable to the radar wavelength causes strong scattering of the signal. This scattering would make it

impossible to detect any target below the regolith, as echo strength would be weakened by several tens of decibels (dBs).

In spite of all these uncertainties, experience has shown that data such as those presented in Table 1 can be used to evaluate radar performance with sufficient accuracy. At the time in which the MARSIS and SHARAD radar sounding experiments were proposed, radar sounding of planetary bodies was deemed problematic if not impossible, in spite of data obtained by the Apollo Lunar Sounder Experiment (ALSE) onboard the Apollo 17 spacecraft [39]. However, results at Mars (e.g., [40]–[43]) have conclusively demonstrated that this technique is effective in the investigation of planetary bodies from orbiting satellites.

V. DESIGN OF THE SUBSURFACE RADAR INSTRUMENT

In this section, we discuss the major design issues of the SSR instrument. The most important issue is related to the choice of the central frequency and of the bandwidth of the radar, which affect its penetration capability, the vertical resolution, and the SNR. The problems of the surface clutter and the signal processing techniques necessary for optimizing the ground resolution of the instrument are also discussed.

A. Central Frequency and Bandwidth

The performance of a radar sounder is determined by two fundamental parameters, namely frequency and bandwidth. Radar frequency determines the penetration capability of the radar, while bandwidth of the transmitted pulse determines range resolution [46].

The number of wavelengths that an electromagnetic wave can penetrate into natural materials before being attenuated to a given fraction of its initial amplitude is approximately the same regardless of radar frequency. This is because dielectric losses (loss tangent) in most natural materials are independent of radar frequency over a wide range of frequencies ranging from megahertz to gigahertz and beyond. This can be verified through examination of the following approximate expression of the one-way attenuation [3]:

$$
\begin{aligned}
\alpha &= 129\sqrt{\varepsilon_R}\, f \left[\sqrt{1 + \tan^2 \delta} - 1\right]^{\frac{1}{2}} \\
&\approx 91\sqrt{\varepsilon_R}\, f \tan \delta \\
&\approx 1.6\sigma/\sqrt{\varepsilon_R} \ \text{dB/km}
\end{aligned}
\tag{1}
$$

where ε_R is the relative dielectric permittivity of the material through which the pulse propagates, f is the radar carrier frequency in megahertz, $\tan \delta$ is the loss tangent, and σ is the conductivity of the medium (in μSm^{-1}). This approximate equation is valid for nonmagnetic media with a low loss tangent. From [47], one can see that attenuation is directly proportional to the radar frequency, and that losses are directly proportional to the conductivity of the medium. It has been shown that the imaginary part of the dielectric constant of pure water ice is almost inversely proportional to the radar frequency in the range between few megahertz and hundreds of megahertz. Thus, the conductivity is almost constant. This behavior has been shown valid for a very wide temperature range 190–278 K [3], [47]. This means that, for a pure ice, attenuation is frequency independent. Despite the fact that the frequency range in which this behavior is observed decreases with temperature, we expect that it can be observed at the very low temperature of the icy moons of Jupiter. Thus, deep penetration requires that the radar operates at the lowest possible frequency.

In most orbiting radars, range resolution is not achieved through the transmission of the shortest possible pulse, but rather through the use of a chirp, i.e., a long pulse that is linearly modulated in frequency. In this case, the vertical (range) resolution of the radar sounder ρ_z is equal to

$$
\rho_z = \frac{c}{2B_w\sqrt{\varepsilon_R}}
\tag{2}
$$

where B_w depicts the radar bandwidth and c is the speed of light. Thus, it can be seen that penetration and resolution are conflicting requirements, as the bandwidth cannot be larger than the highest frequency. A tradeoff between these opposite constraints has to be found in the radar design. It is important to note that the bandwidth of the signal is a key factor also for the gain of the system. Indeed, radar systems using chirp signals can exploit the so-called range compression processing, obtaining a processing gain equal to

$$
\eta_z = \tau B_w
\tag{3}
$$

where τ represents the chirp duration. The value of η_z is typically in the order of 25–30 dB.

As discussed above, the frequency dependence of attenuation requires that subsurface sounding radars operate at low frequency (< 100 MHz) in order to achieve a deep penetration. The choice of the radar frequency affects also instrument characteristics, and especially the size of the antenna. The exact choice of the radar frequency results from a tradeoff between science requirements and technical limitations. In greater detail, we need to jointly analyze the need to achieve deep penetration with respect to the effect of the Jupiter radio noise, the crust attenuation, surface and volume scattering, and the limitations in power and antenna size.

B. Signal-to-Noise Ratio

The dynamic range of the radar, i.e., its capability to detect weak echoes, is limited by the presence of radio emission from natural sources. In order to estimate the SNR for the received echoes, all the sources of noise included in the acquisition process should be analyzed and modeled. In our case, we should consider: 1) the thermal noise (which is a typical noise in radar systems due to electronic devices); 2) the galactic noise; and 3) the Jovian radio emission. The strongest noise component for the JGO subsurface radar is the Jovian radiation emission, which is peculiar of this kind of mission (see Section IV-A). For this reason, we focus our attention on this component.

From Fig. 5, one can see that the electromagnetic flux density from Jupiter at 1 AU at a frequency of about 10 MHz is in the order of -200 dBWm^{-2}Hz^{-1} on average, climbing to -190 dBWm^{-2}Hz^{-1} in periods of intense activity and reaching peak intensities of up to -180 dBWm^{-2}Hz^{-1}. Scaling for the distance of Ganymede from Jupiter (mean distance 1 070 400 km), flux densities become -157 dBWm^{-2}Hz^{-1}, -147 dBWm^{-2}Hz^{-1}, and -137 dBWm^{-2}Hz^{-1}, respectively. By comparison, galactic emission at the same frequency provides an electromagnetic flux density in the order of -190 dBWm^{-2}Hz^{-1} [48], thus more than 30 dBWm^{-2}Hz^{-1} below the average level of the Jovian flux. Thus, it is obvious that Jupiter radio noise is one of the main critical issues to consider for evaluating the capability of SSR to detect subsurface echoes. Several approaches are possible to mitigate the problem (e.g., proper choice of the carrier frequency, definition of the acquisition strategy, choice of the pulse duration, and repetition frequency) and a combination of them will probably be required to meet the instrument scientific goals.

An analysis of Fig. 5 reveals that radio noise decays very rapidly with increasing frequency above 10 MHz, by at least one order of magnitude before reaching 100 MHz. The exact shape of the spectrum in this range of frequencies is critical in determining the choice of the operating frequency for the radar, because of the requirement of penetration in the Ganymedean crust, which drives the selection towards lower frequencies. As mentioned in Section IV-A, the frequency cutoff for the Jovian radio emission affecting the subsurface radar is around 40 MHz.

In theory, it is possible to avoid radio bursts that have the capability to blind the radar. However, while the pattern of activity is known on average, sporadic events are not predictable, thus making any strategy for avoiding extreme events highly unreliable. Another option could be to operate the radar on the anti-Jovian side of Ganymede only, using the disk of the moon to shield the instrument from the Jovian radio emission. This choice would leave galactic noise as the only external contribution to instrument noise, but it would result in the observation of less than half of the surface of the moon, as Ganymede is in synchronous rotation around Jupiter.

A possible technical option to reduce the effects of the Jupiter radio noise is the use of an antenna with high directivity and high gain, as an array of dipoles. However, the long wavelength at which the radar is expected to operate (of the order of 6–30 m) makes the implementation of this kind of antenna very challenging from a mechanical viewpoint taking into account the need of a deployment procedure. Thus, this solution at the present is not considered feasible for SSR due to technical constraints of JGO. The MARSIS radar is equipped with a secondary monopole antenna that has a null in the nadir direction, thus being capable of detecting lateral surface echoes, but not nadir subsurface echoes. The same system could in principle be used to cancel emission arriving from Jupiter, but experience has shown that the position of the null is strongly dependent on the shape and orientation of conducting spacecraft parts, which have a size comparable to the wavelength, because of their interactions with the electric field emitted by the antenna. Making an antenna with a null in a controlled direction would thus impose very strict constraints on spacecraft design, which are not realistic in the considered mission. There are other techniques that would allow the radar to operate in a noisy environment, such as, for example, the use of circularly polarized signals. However, this method would require at least a cross dipole antenna, and would thus significantly increase the complexity of the instrument design and of its accommodation on the spacecraft.

C. Signal-to-Clutter Ratio

As briefly mentioned in Section V-A, another important factor affecting the performance of the radar is clutter, which consists of off-nadir surface reflections reaching the radar at the same time as subsurface nadir reflections, thus potentially masking them. In the current baseline option, SSR is expected to operate in the frequency range between 10 and 50 MHz. At these wavelengths, mass, volume, and mechanical constraints in space missions make dipoles, which have negligible directivity, the most suitable antennas. Thus, when transmitting, the radar illuminates the entire surface of the observed body, and areas of the surface that are not directly beneath the radar can scatter part of the incident radiation back towards it, producing surface echoes that will reach the radar after the echo coming from nadir. As subsurface echoes will also reach the radar after the nadir surface reflections, it becomes difficult to separate the two contributions. This is particularly true in the across-track direction. Indeed, in the along-track direction clutter can be reduced by means of synthetic aperture processing (see Section V-D). A schematic example of the surface clutter problem is presented in Fig. 2.

The strength of clutter is controlled by statistical parameters of the topography of natural surfaces scattering the radiation. Parameters such as root mean square (RMS) height, RMS slope, or correlation length are used in radar
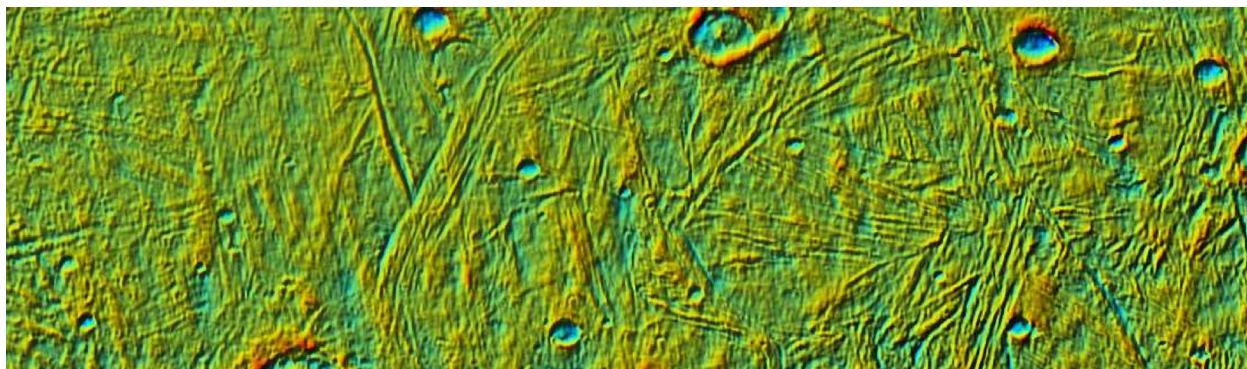
Fig. 8. *Shaded relief visualization of the digital elevation model produced by Kirk [49] through stereogrammetry from Voyager 2 images 20638.45 and 20638.53, for an area of Ganymede located around 120° W, 20° S. The DEM consists of 1110 lines of 320 samples each, with a 629-m resolution. Maximum elevation is 1748 m, and minimum is −2261 m. The majority of topographic height values comprises the range between −500 and 500 m.*

backscattering models (e.g., see [50]) to estimate clutter strength and to compare it with the intensity of subsurface reflections. The SCR is thus computed to estimate the capability of the radar to detect a subsurface echo at a given depth (e.g., see [51]). The aforementioned parameters are essentially unknown for Ganymede, at least at the scales which are relevant for scattering in the 10–100-MHz range, which range between few meters and a hundred meters. Some topographic information has been derived for a limited number of areas through stereogrammetry from Galileo [52] and Voyager [53] images. Schenk [54] has computed values of RMS slope for Europa using Galileo and Voyager data, obtaining values between 10° and 15° at 10–100-m length scales, which are much steeper than those of typical landing sites on Mars. Some information for Ganymede was obtained through a digital elevation model (DEM) produced from Voyager images made available by Kirk [49]. This DEM is shown in Fig. 8. It is centered approximately at 120° W, 10° S on light grooved terrain, which is one of the roughest geologic units on Ganymede. It covers an area of ∼200 × ∼700 km^2 at ∼630-m/pixel resolution. The derived RMS slope is of about 5.5°, which, from the clutter point of view, is more favorable than the 10–15° derived for Europa and consistent with data points for Ganymede presented in [54]. This value is comparable to values found in the southern highlands of Mars [55]. However, more work is necessary for deriving DEMs of different portions of Ganymede for a better understanding of the clutter issue.

D. Ground Resolution and Synthetic Aperture Processing

In order to satisfy the scientific goals of SSR a minimum ground resolution of 1×5 km^2 (along × across track) has been identified (see Section II). The resolution of the system depends on many factors, such as the antenna pattern, the orbit height, and the surface roughness.

As mentioned in the previous section, due to the complexity of the antenna deployment, a dipole antenna has been selected as baseline for SSR, exploiting and developing the heritage from the radar sounders presently operating at Mars [6], [56]. The choice of a dipole antenna implies that for a central frequency in the order of 10–50 MHz the antenna must have a size between 30 and 6 m. The precise antenna length will depend on the adopted central frequency and on the antenna matching technique. At the time of writing, a 10-m dipole antenna is the baseline for SSR.

As an example, the ideal radiation pattern of a dipole with length L_a comparable to the signals wavelength λ ($L_a = 0.8\,\lambda$) is shown in Fig. 9. This ideal model is only an approximation of the real radiation pattern. Indeed, as mentioned in Section V-B, the experience from other radar sounder experiments shows that the real pattern is significantly affected by all the structures of the spacecraft that have an electromagnetic interaction with the dipole. Considering the case in which the antenna is oriented along the JGO track, the pattern has thus a single lobe on the plane parallel to the track direction (along track), and it is isotropic on the across-track plane. Therefore, the antenna footprint is limited by the antenna beam in the along-track direction and only by the Ganymede radius in the across-track direction. This situation is described in Fig. 10. The size of the antenna footprint on the ground is given by

$$\rho_{\mathrm{alt}} = h\theta_{3\,\mathrm{dB}} \approx \frac{h\lambda}{L_a} \qquad (4)$$

$$\rho_{\mathrm{act}} = R_G(\pi - 2\theta_{\mathrm{act}}) \qquad (5)$$

where ρ_{alt} represents the footprint size in the along-track direction [57]; ρ_{act} is the footprint size in the across-track
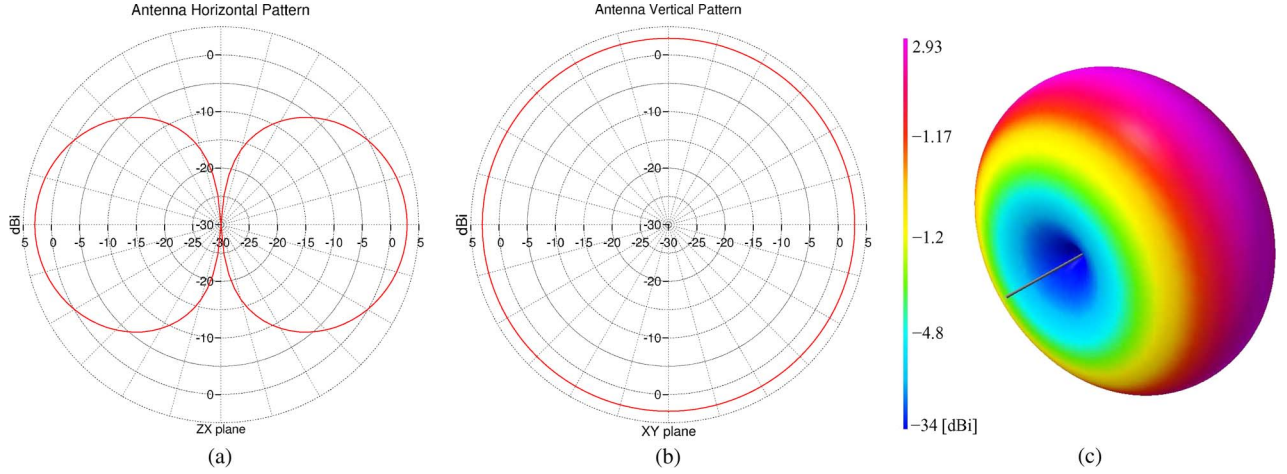
Fig. 9. *Ideal radiation pattern of a dipole with antenna length $L_a = 0.8\lambda$. (a) Horizontal plane, i.e., any plane containing the dipole axis; (b) vertical plane, i.e., the plane perpendicular to the dipole axis and containing the dipole center; (c) 3-D representation; the dipole is depicted by the gray segment.*

direction; h is the orbit height; $\theta_{3\,\text{dB}}$ is the 3-dB aperture of the antenna; R_G is the radius of Ganymede; and $\theta_{\text{act}} = \arcsin(R_G/(h + R_G))$ is the angle between the nadir direction and the tangent to the moon's surface passing through the orbiter position [see Fig. 10(b)]. For example, assuming $L_a = 0.8\lambda$, $h = 200$ km, and $R_G = 2634$ km, we obtain $\rho_{\text{alt}} = 250$ km and $\rho_{\text{act}} = 1991$ km. The broadness of the dipole radiation pattern results in a very large ground footprint. However, the real along- and across-track resolutions of the radar are better than the ground footprint and are calculated as follows.

1) Along-Track Resolution: In the along-track direction, it is possible to exploit the Doppler effect and thus a synthetic aperture to improve the ground resolution. As a result, the surface contributions coming from off-nadir in the along-track direction are reduced, thereby improving also the SCR. As the spacecraft is moving along its orbit, an ideal point target on the ground is illuminated by the radar in a time interval T_i (called integration time) given by

$$T_i = \frac{\theta_{3\,\text{dB}}h}{V_s} \qquad (6)$$

where V_s is the velocity of the spacecraft (for simplicity, we assume it is equal to 2 km/s by ignoring the small difference between spacecraft and ground velocities). During the integration time the target response shows different
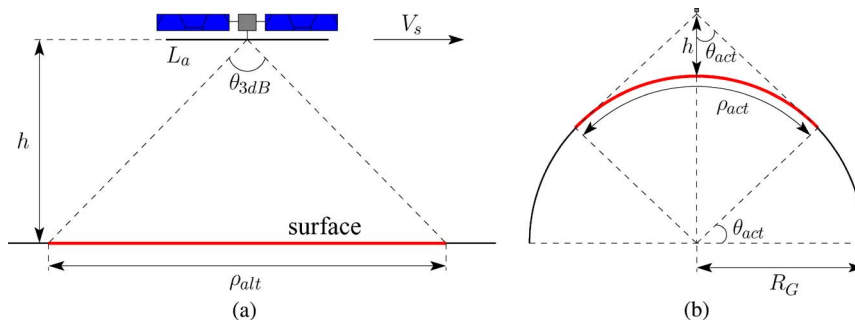

Fig. 10. *Acquisition geometry of SSR in the along- and across-track planes in the case the dipole antenna is oriented in the along-track direction. In the along-track direction, the antenna ground footprint is thus limited by the width of the antenna main radiation lobe. In the across-track direction, the ground footprint is limited only by the moon's radius, as the antenna radiation pattern in the across-track plane is isotropic (see Fig. 9). (a) Along-track plane: h indicates the orbit altitude, L_a is the dipole length, $\theta_{3\,\text{dB}}$ represents the 3-dB aperture of the antenna, V_s is the speed of the spacecraft, and ρ_{alt} represents the along-track antenna aperture on the ground; (b) across-track plane: R_G is the radius of Ganymede, θ_{act} indicates the angle between the nadir direction and the tangent to the moon's surface passing through the orbiter position, and ρ_{act} represents the antenna aperture on the ground in the across-track direction.*

Doppler shifts due to the relative motion of the spacecraft with respect to the target. Therefore, although different targets are present in the same antenna footprint, their returns have different Doppler shifts. As SSR is a coherent radar, it measures and records the phase history of the received signals. This information can be exploited to resolve the ground targets in the Doppler domain using a focusing algorithm, which analyzes the phases of a series of consecutive echoes.

The Doppler processing can be *focused* or *unfocused*. The choice of the focusing strategy for SSR has to take into account the processing requirements, the data rate, the SNR gain produced by each strategy, and the power consumption and supplementary mass involved by additional onboard processing. These parameters will compete in a tradeoff between the instrument constraints and the scientific goals of the mission. At the present status of the study, the power budgets of the possible processing configurations have been only roughly estimated and only general comments are possible on this issue. On the contrary, mass estimates indicate that all the processing options should fit in the 10 kg currently allocated for the SSR instrument. In the following, we describe the main processing options under study for SSR.

a) Focused processing: In the focused case the phase history of the signal is fully exploited and the maximum theoretical along-track resolution that is achievable is in the order of few meters. The result of the focusing algorithm is the synthesis of a long antenna (i.e., synthetic antenna or synthetic aperture), which length is equal to the space covered by the orbiter during the integration time. In general, the synthetic antenna length L_s is given by

$$L_s = T_i V_s. \qquad (7)$$

The resulting aperture is much longer than the physical one. This is possible if the Doppler shifts are properly sampled by the instrument pulse repetition frequency (PRF). The lower limit to the PRF is thus given by the total Doppler bandwidth B_D, which is equal to [58]

$$B_D = \frac{2V_s^2}{h\lambda} T_i. \qquad (8)$$

The along-track resolution obtained after the focusing (ρ_{alt}) can be calculated as follows [58]:

$$\rho_{alt}^f \approx \frac{V_s}{B_D} = \frac{h\lambda}{2L_s}. \qquad (9)$$

Equation (6) indicates the maximum ideal integration time. However, for space-borne radar sounders it is commonly assumed that the coherent scattering from the ground is limited by the first Fresnel zone. The diameter of the Fresnel zone D_F is given by

$$D_F = \sqrt{2\lambda h}. \qquad (10)$$

As an example, considering a carrier frequency of 50 MHz ($\lambda = 6$ m) and an orbiter altitude of 200 km, the value of D_F is 1549 m. The integration time can be thus reduced to match a ground surface with a length equal to D_F, obtaining

$$T_{i,eff}^f = \frac{D_F}{V_s} \qquad (11)$$

where $T_{i,eff}^f$ is called effective integration time. From (7), this is equivalent to set a synthetic aperture length equal to D_F. The along-track resolution calculated using the effective integration time is thus lower than the maximum value that it is possible to achieve in the ideal case. In the considered example, one obtains that the processed Doppler bandwidth is $B_D = 5.16$ Hz, corresponding to $\rho_{alt}^f \approx 387$ m, which is well below the limit imposed by the instrument design constraints.

The number N of echoes that should be processed to obtain the fixed synthetic aperture is

$$N = T_{i,eff}^f \mathrm{PRF}. \qquad (12)$$

Generally, a PRF much higher than the lower limit imposed by the Doppler bandwidth is used to improve the SNR. For instance, using PRF = 500 Hz, the number of echoes is $N = 387$. Such echoes are integrated to focus one resolution cell. As a consequence, the SNR of the focused signal increases by a factor N. In the considered case, the SNR increment is thus equal to approximately 26 dB. This gain is called azimuth compression factor η_a.

Despite the many advantages of the focused Doppler processing, it is highly resource demanding with respect to the power budget if implemented onboard. Moreover, a very robust focusing algorithm must be implemented in order to deal with possible different acquisition scenarios. Indeed, if only the focused data are transmitted to Earth, it is not possible to run again the focusing processing (e.g., changing the parameters of the algorithm) as the raw data are not more available. A solution to these problems could be to avoid onboard processing and directly downlink to

the Earth the raw data. The focusing step could be then performed offline on the ground segment. However, this option could also imply that a large amount of data should be transmitted to the ground segment. Present estimates indicate that the raw data rate is of about 13 Mb/s. Due to the very limited downlink data rate per instrument foreseen for JGO, the transmission of such amount of data is not feasible and some (partial) processing has to be done onboard in order to reduce the instrument data rate. A reduction factor of 30–35 with respect to the raw data rate can be achieved by performing echo presumming and range compression onboard. The resulting data rate would be in the order of 400 kb/s.

b) Unfocused processing: The unfocused Doppler processing permits to reduce the computation effort of the onboard electronics with respect to the focused case at the cost of a reduced along-track resolution. Following the MARSIS approach [5] (i.e., requiring that the signal phase variation during a synthetic aperture is smaller than $\pi/4$), the phase compensation of the echoes during the formation of a synthetic aperture is simpler and can be performed onboard in real time, as only a linear phase compensation of the echoes is required. Under such condition, the maximum antenna aperture is

$$L_s = \sqrt{\frac{h\lambda}{2}} \qquad (13)$$

which, from (7), corresponds to a an effective integration time $T_{i,\text{eff}}^{uf}$ given by

$$T_{i,\text{eff}}^{uf} = \frac{1}{V_s} \sqrt{\frac{h\lambda}{2}}. \qquad (14)$$

By inserting (13) in (9), one obtains that the along-track resolution in the unfocused case ρ_{alt}^{uf} is equal to the synthetic antenna length L_s. Therefore, the algorithm needs to process only one aperture per resolution cell and subsequent apertures do not overlap. This results in a further reduction of the computation effort for the digital section of the instrument in the case of onboard processing. For the example considered in this section, from (9), it results $\rho_{\text{alt}}^{uf} \approx 775$ m. This value is still compatible with the instrument design specifics. Unfortunately, as the synthesized aperture is shorter than in the case of focused processing, the processing gain is lower. Inserting (14) in (12), one obtains $\eta_a = N = 193$, corresponding to an SNR gain of approximately 23 dB. The data rate achievable with this technique is in the order of 150 kb/s. Due to the additional electronics with respect to the presumming-only option discussed in the previous paragraph, an increment

in the order of 30% of the power consumption is expected.

2) Across-Track Resolution: For the across-track direction, no Doppler processing is possible. In fact, in the across-track plane the spacecraft has no relative motion with respect to the ground targets and thus the backscattered signals have no Doppler shift. However, although the antenna radiation pattern is isotropic the echoes coming from large off-nadir angles can be assumed to be sufficiently weak to not affect the echoes coming from nadir direction when the surface is flat. On the one hand, for smooth surfaces, the across-track ground resolution ρ_{act} is assumed to be equal to the first Fresnel zone diameter (10). On the other hand, for the case of incoherent scattering (rough surface) the ground resolution is commonly approximated with the so-called first pulse-limited resolution cell (D_{pl}). The first pulse-limited cell is represented by a circle on the ground centered in the nadir point, which diameter is given by the intersection of the wavefront with the ground surface when the transmitted wave has penetrated into the ground to a depth equal to ρ_z (see Fig. 2). The diameter of such a circle is given by

$$D_{pl} = 2\sqrt{2h\rho_z} = 2\sqrt{\frac{hc}{B_w}}. \qquad (15)$$

Considering a bandwidth $B_w = 10$ MHz, in the rough surface case the value of the across-track resolution results in $\rho_{\text{act}} = D_{pl} = 4899$ m. The across-track resolution is thus in the range defined by the instrument specifics.

VI. PROCEDURE FOR PERFORMANCE ASSESSMENT

In the previous sections, we discussed the main issues and components that should be considered in the design of the JGO subsurface radar. All these components should be jointly analyzed for defining a system that can achieve the performance necessary for satisfying the scientific objectives. To this aim, a suitable SSR instrument performance model has been developed. The architecture and input and output variables of this model are shown in Fig. 11.

For a nadir-looking subsurface sounder the most important performance figure is related to its penetration capability that depends on the power ratio between the signal coming from a generic subsurface interface (a change in the dielectric constant) and, generally speaking, noise coming from all disturbing and unwanted signal sources. Therefore, as shown in Fig. 11, an evaluation of the signal power requires proper models for characterizing
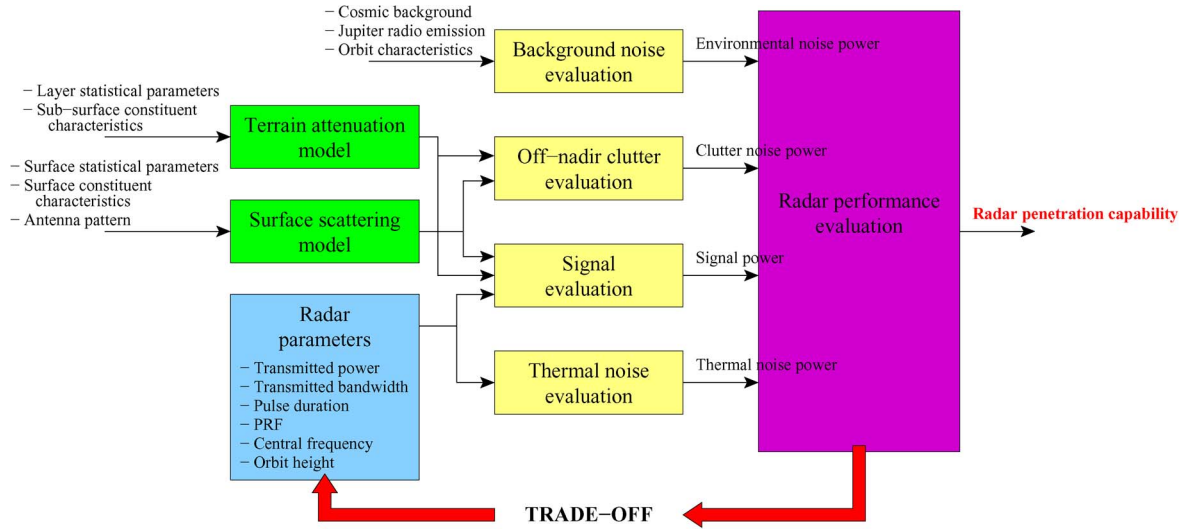
Fig. 11. *Instrument performance model.*

surface and subsurface scattering and propagation, as well as the analysis of the main system parameters, such as transmitted bandwidth, central frequency, pulse duration, PRF, antenna pattern, antenna gain, and transmitted power.

The moon's surface roughness can be characterized by assigning a statistic behavior that implies an electromagnetic backscattering function, while subsurface is handled through a suitable model for electromagnetic attenuation and propagation. Noise power evaluation takes into account off-nadir clutter, thermal noise, and background sources, such as Jovian and galactic noise. In order to easily identify and adequate tradeoff among the system parameters, final instrument penetration capability is evaluated by using only analytical expressions. Some details on this procedure are reported in the following.

Signal power P_r can be evaluated by using a classical radar equation for monostatic systems that expresses the received power by the radar as a function of the transmitted power P_t, the antenna gain G, the wavelength λ, the radar altitude h, and the target radar cross section. Taking into account the scattering from the moon surface, we obtain

$$P_r(\theta) = A\sigma_s(\theta) \qquad (16)$$

$$A = \frac{P_t \lambda^2 G^2}{(4\pi)^3 h^4} \qquad (17)$$

where σ_s represents the surface radar cross section and θ depicts the radiation incidence angle. σ_s can be expressed by the product of surface backscattering coefficient σ_0 and

illuminated area that, as described in Section V-D2, can be approximated by the pulse-limited circle (15), i.e.,

$$\sigma_s(\theta) = \pi \left(\frac{D_{pl}}{2} \right)^2 \sigma_0(\theta). \qquad (18)$$

Ganymede and Callisto terrains are supposed to be a random rough process. A fractal geometry is considered as it has been proved [59] to be a suitable method for describing natural surfaces. One important advantage of fractal parameters is that, unlike classical statistical parameters, they are independent from the observation scale. The most suitable fractal model is the fractional Brownian motion (fBm), which is a stochastic nonstationary process described in terms of the probability function of its increments. Height differences of an fBm surface have a Gaussian probability density function whose standard deviation (σ_{fBm}) depends on the distance between points (ν), i.e.,

$$\sigma_{\text{fBm}} = s\nu^H \qquad (19)$$

where H is the Hurst coefficient $(0 < H < 1)$ and s is the standard deviation of surface increments at unitary distance related to an fBm characteristic length. Such characteristic length is called topothesy (Φ) and is related to s as follows:

$$s = \Phi^{1-H}. \qquad (20)$$

Since the surface mean square deviation is equal to the mean square deviation of the surface increments divided by ν, the topothesy can be interpreted as the distance over which chords joining points on the surface have a surface slope mean square deviation equal to unity. In this way, a closed form for the backscattering coefficient can be derived with the Physical Optics (PO) solution under the Kirkhhoff Approximation (KA) [60]

$$\sigma_0(\theta) = 2k^2 \rho'(\theta) \cos^2 \theta$$
$$\times \int_0^\infty J_0(2kt|\sin\theta|) \exp(-2s^2 k^2 t^{2H} \cos^2 \theta) t\, dt \quad (21)$$

where $k = 2\pi/\lambda$ is the wavenumber, and $\rho'(\theta)$ is equivalent to the Fresnel power reflection coefficient in the limit as the surface becomes perfectly smooth

$$\rho'(\theta) = \left| \frac{\cos\theta - \sqrt{\varepsilon'_R - \sin^2\theta}}{\cos\theta + \sqrt{\varepsilon'_R - \sin^2\theta}} \right|^2 \quad (22)$$

where ε'_R is the surface relative permittivity. The expression for the backscattering coefficient given in (21) shows similarities to other models for particular values of H. For instance, when $H = 0.5$, the backscattering coefficient becomes similar to Hagfor's law [61], while when $H = 1$, the backscattering coefficient coincides with that obtained in the case of very rough classical surfaces with Gaussian probability density function and Gaussian correlation function [60].

When signal power coming from a subsurface at depth z is evaluated, the transmission coefficient of the first interface, the attenuation of the crossed terrain layer and the subsurface radar cross section should be considered. These terms can be included in the following factor

$$\Gamma = [1 - \rho'(0)]^2 \sigma_{ss}(0) \exp(-\alpha_{TOT}) \quad (23)$$

where σ_{ss} is the subsurface radar cross section that has an equation similar to (18) but considering different Fresnel power reflection corresponding to the subsurface layer with relative permittivity ε''_R

$$\rho''(\theta) = \left| \frac{\sqrt{\varepsilon'_R}\cos\theta - \sqrt{\varepsilon''_R - \varepsilon'_R \sin^2\theta}}{\sqrt{\varepsilon'_R}\cos\theta + \sqrt{\varepsilon''_R - \varepsilon'_R \sin^2\theta}} \right|^2. \quad (24)$$

The power received from subsurface backscattering is thus equal to $A\Gamma$. It is worth noting that (23) gives an optimistic evaluation of power passing trough first interface along nadir direction ($\theta = 0$) since it uses, as transmission coefficient, the factor $[1 - \rho'(0)]$ that is strictly correct only for flat surfaces.

α_{TOT} is the total two-way attenuation of terrain layer, given by

$$\alpha_{TOT} = 2 \int_0^z \alpha(l)\, dl. \quad (25)$$

As discussed in Section IV-B, models for estimating the expected attenuation as a function of ice depth on Jupiter's icy moons are available in the literature. For example, a model has been developed by Chyba *et al.* [33] for evaluating attenuation of Europa's ice. The model takes into account percentage and kind of ice intrusion and the final ice attenuation is strongly dependent on ice temperature. Chyba *et al.*'s model can be adapted to Ganymede by considering a different range of temperature as a function of the ice depth. In the following examples, we consider a surface temperature of 120 K and a slow linear increasing with depth of about 10 K within the first 5-km depth [29]. With this temperature profile and by considering lunar dust impurities ($\varepsilon_R = 2.4$) [33] concentration of 5%, it is possible to obtain ice attenuation values as a function of penetration depth for different carrier frequencies. Fig. 12 shows the attenuation values as a function of depth for 20- and 50-MHz radar central frequency.
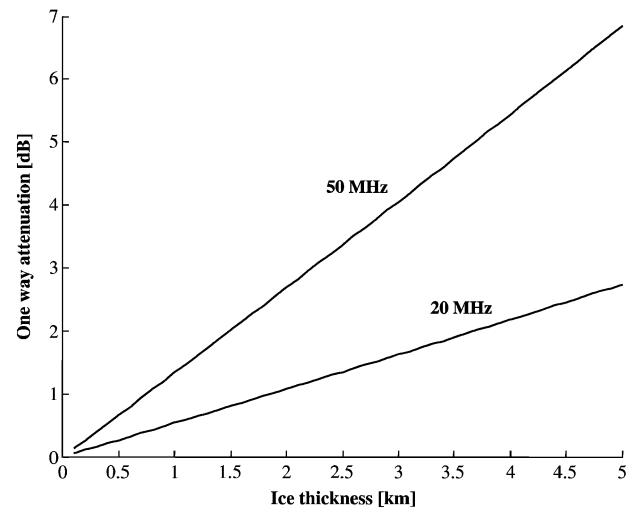

Fig. 12. *One-way ice attenuation based on Chyba et al. model [33]. Temperature varying linearly with depth from 120 up to 130 K. Lunar dust impurities ($\varepsilon_R = 2.4$) concentration of 5%.*

For signals also compression factor in either range and along track should be considered, taking into account coherent integration, which improves the SNR. Thus, we define the total compression factor η as follows:

$$\eta = \eta_z \eta_a. \tag{26}$$

As far as noise is concerned, contributions arise from thermal noise, environmental noise, and surface clutter. Each term contributes to a different SNR definition (see Section IV). Thermal noise is defined as follows:

$$N_{th} = k_B T_s B_w F \tag{27}$$

where k_B is the Boltzmann constant, T_s is the system temperature, and F is the receiver noise figure. From (16), (23), (26), and (27), the expression of the SNR related to thermal noise is thus given by

$$\mathrm{SNR}_{th} = \frac{A\Gamma\eta}{N_{th}}. \tag{28}$$

Jupiter radio emission noise and galactic noise have been already discussed in Sections IV-A and V-B. These effects can only be mitigated by the antenna pattern and depend on orbit characteristics and satellite attitude. Jovian noise is the most relevant noise component. This environmental radio noise is strongly different from that experienced on Mars as the classic galactic noise is sharply below the Jupiter radio emission. As mentioned in Section V-B, in the anti-Jovian part of the orbit around Ganymede, the Jovian radio emission is masked by the moon disk and thus it becomes negligible. Therefore, by considering an equivalent noise temperature for both Jupiter (T_J) and galactic (T_g) radio noises, the noise contribution in the Jovian (N_J) and anti-Jovian part (N_{AJ}) of the orbit can be estimated as

$$N_J = k_B T_J B_w F W_J + k_B T_J B_w F \bar{\rho} W_G \tag{29}$$
$$N_{AJ} = k_B T_g B_w F \tag{30}$$

where the first term of N_J is due to the direct radiation from Jupiter and is weighted by the antenna pattern in the Jupiter direction W_J, while the second term is due to the reflection on the surface of Ganymede of the direct radiation from Jupiter. This last term depends on both the Ganymede surface reflectivity (albedo) $\bar{\rho}$, which is about

0.07 for $\varepsilon'_R = 3$, and the antenna pattern in the expected reflection directions W_G.

For instance, at 20 MHz, the equivalent noise temperature for the galactic noise is about 65×10^3 K, while that for Jovian noise is about 2×10^8 K, corresponding to a power flux of -147 dBWm^{-2}Hz^{-1} [14]. It is worth noting that direct Jupiter radio emission comes from a very narrow angular region over the planet's poles (about $1°$ [14]), while the reflected part, even if weighted by surface reflectivity, comes from a very wide angular region (about $136°$ at 200-km altitude). Preliminary results for ideal antenna pattern (in the worst case of Jovian noise along the antenna gain maximum direction) give $W_J = 0.02$ and $\bar{\rho}W_G = 0.07$. It is worth noting that either equivalent noise temperature for galactic and Jovian noise are orders of magnitude greater than system temperature (in the order of 300 K). For this reason, thermal noise can be neglected in the evaluation of instrument overall performance.

The corresponding SNRs are given by

$$\mathrm{SNR}_J = \frac{A\Gamma\eta}{N_J} \tag{31}$$

$$\mathrm{SNR}_{AJ} = \frac{A\Gamma\eta}{N_{AJ}}. \tag{32}$$

The basic equation for evaluating the SCR is given by [62], [63]

$$\mathrm{SCR} = \frac{A\Gamma}{P_r(\bar{\theta})} \tag{33}$$

where

$$\bar{\theta} \approx \sqrt{\frac{2z\sqrt{\varepsilon'_R}}{h}}. \tag{34}$$

In order to evaluate all the aforementioned contributions in a single term, the total SNR is calculated as follows:

$$\mathrm{SNR}_{\mathrm{TOT}} = \left(\frac{1}{\mathrm{SNR}_{th}} + \frac{1}{\mathrm{SNR}_{J/AJ}} + \frac{1}{\mathrm{SCR}} \right)^{-1} \tag{35}$$

where the term $\mathrm{SNR}_{J/AJ}$ is given by (31) or (32) depending on the considered part of the spacecraft orbit.

Fig. 13. *SNR values for a carrier frequency of 50 MHz. The subsurface dielectric constant is $\varepsilon_R'' = 4$. A first layer of ice with attenuation as shown in Fig. 12 is considered.*
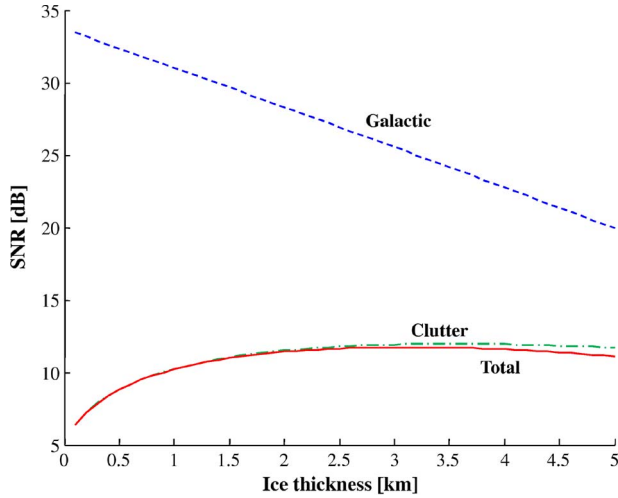

Fig. 14. *SNR values for a carrier frequency of 20 MHz. The subsurface dielectric constant is $\varepsilon_R'' = 4$. A first layer of ice with attenuation as shown in Fig. 12 is considered.*
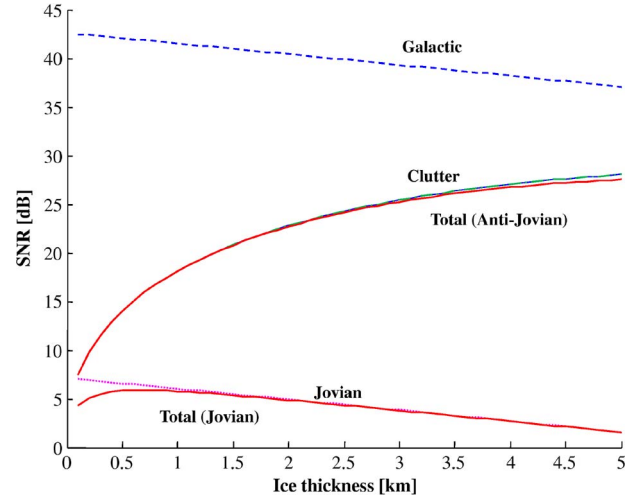
As an example, in order to better illustrate various effects of radar parameters on overall performance and possible tradeoffs, in the following, we report a preliminary (and simplified) radar definition and evaluation of performance. To this aim it is supposed to have a quite rough surface, as suggested by the available DEM (see Section V-C), and a smooth subsurface with low contrast ($\varepsilon_R'' = 4$). Higher values of dielectric constant for the subsurface, corresponding to basalt-like bedrock ($\varepsilon_R'' = 7$) and liquid water ($\varepsilon_R'' = 87$), do not seem possible within the first 5-km ice depth [29]. The used fractal parameter values are $H = 0.5$, $\Phi = 0.1$ for the surface, and $H = 0.5$, $\Phi = 0.01$ for the subsurface. These values should be considered as a first example in order to address the influence of surface statistical parameters on achievable SNR and, thus, on final instrument penetration capability. Such values need to be confirmed through measures on available Ganymede's DEMs.

Being the Jovian radio emission the most critical source of disturbing signal and taking into account its behavior as a function of frequency (see Fig. 5), the choice of the central frequency is oriented on high values of the range under investigation (between 10 and 50 MHz) also taking into account that ice attenuation is almost constant up to hundreds of megahertz. For example, for a carrier frequency of 50 MHz, Fig. 13 shows the expected values of $\mathrm{SNR_{TOT}}$ versus the ice thickness. In this case, being only present galactic noise, the instrument performances are essentially limited by clutter. As shown in Fig. 14, the situation is different for the 20-MHz case. In this case, in the Jovian part of the orbit the Jupiter radio emission is the noise factor that limits the overall instrument performance. $\mathrm{SNR_{TOT}}$ values improve significantly in the anti-Jovian part of the orbit where only the galactic noise (and

of course clutter) affects the penetration capability of the radar. In this last case, the $\mathrm{SNR_{TOT}}$ values achieved with the 20-MHz carrier are much higher than those obtained at 50 MHz since, as expected, off-nadir clutter decreases by decreasing the value of carrier frequency.

An important role in the evaluation of the system performance is also played by the choice of the PRF and pulse duration values, which can significantly increase the overall SNR and thus improve the radar detection capability. In the aforementioned examples, a PRF of 500 Hz and a pulse duration τ of 150 μs have been considered. The antenna length has been set to $L_a = 0.8\lambda$ for both carrier frequencies.

VII. DISCUSSION AND CONCLUSION

In this paper, after a general overview of the EJSM, we have addressed the challenging problem of defining and designing the SSR instrument included in the model payload of the JGO. From the presented analysis, it should be clear that, even though the SSR instrument is based on the heritage of the Mars missions MARSIS and SHARAD, the Jupiter environment, the properties of the surface and subsurface targets on Ganymede (and Callisto), and the constraints on the available resources (in terms of mass, power, and expected data rate in downlink) make the design of the instrument a complex process.

In this paper, we presented the main scientific goals associated with SSR (also briefly mentioning their synergies with the objectives of the IPR included in the JEO payload and devoted to the exploration of Europa), the major critical issues to be considered in the design of the instrument (i.e., the Jupiter radio emission, the properties of targets, the expected clutter, the geometrical resolution,

the range resolution, the penetration requirements, and the antenna constraints), and the performance model defined for the design of the instrument.

Although at this phase of the mission no final choices have been done on the radar sounder subsystems and parameters, all the aforementioned parts have been illustrated pointing out the main theoretical challenges and providing numerical examples for a better understanding of the different tradeoffs at the basis of the expected performances of the system.

Looking at the most critical issues, at the present the activity is focused on the following directions: 1) refining a model of the Ganymede surface (digital elevation model) and subsurface to be used for optimizing the assessment of the radar performances versus the different parameters settings; 2) improving the understanding of the properties of the Jupiter radio emission for making it possible an effective and precise selection of the central frequency of the radar sounder; 3) addressing the problem of the definition of the digital part of the system, taking into account that, on the one hand, the expected very limited downlink data rate imposes the need of processing onboard; on the other hand, the limited power budget available poses constraints on the demanding power absorption required by

the digital part when a relevant amount of processing onboard is considered.

As a final remark, one critical issue that has not been discussed in the paper (because of being outside the scope of this work), but that should be mentioned, is related to the high total ionization dose expected in the Jupiter environment. This is critical also for Ganymede (even if with a less extent than for Europa), which is heavily affected by proton and heavy ion dose. This increases the complexity related to the realization of the instrument from the viewpoint of the electronic and hardware devices, which should be properly designed for guaranteeing a correct behavior during the entire duration of the mission. This is crucial for the SSR payload, also taking into account that the most important phase of the mission for the subsurface radar is the final one, which is associated with the insertion of JGO in circular orbit around Ganymede. ∎

Acknowledgment

REFERENCES

[1] *Europa Jupiter System Mission NASA/ESA Joint Summary Report*, Jan. 2009. [Online]. Available: http://sci.esa.int/ejsm/

[2] V. Bogorodsky, C. Bentley, and P. Gudmandsen, *Radioglaciology*. Dordrecht, The Netherlands: D. Reidel, 1985.

[3] S. Evans, "Dielectric properties of ice and snow—A review," *J. Glaciol.*, vol. 5, pp. 773–792, 1965.

[4] A. Wielders, "Payload definition document for the EJSM Jupiter Ganymede Orbiter," The Joint Europa-Jupiter Science Definition Team, ESA Doc. SCI-PA/2008.029/CE, 2009.

[5] R. Jordan, G. Picardi, J. Plaut, K. Wheeler, D. Kirchner, A. Safaenili, W. Johnson, R. Seu, D. Calabrese, E. Zampolini, A. Cicchetti, R. Huff, D. Gurnett, A. Ivanov, W. Kofman, R. Orosei, T. Thompson, P. Edenhofer, and O. Bombaci, "The Mars Express MARSIS sounder instrument," *Planetary Space Sci.*, vol. 57, pp. 1975–1986, 2009.

[6] R. Seu, R. J. Phillips, D. Biccari, R. Orosei, A. Masdea, G. Picardi, A. Safaenili, B. A. Campbell, J. J. Plaut, L. Marinangeli, S. E. Smrekar, and D. C. Nunes, "SHARAD sounding radar on the Mars Reconnaissance Orbiter," *J. Geophys. Res.*, vol. 112, 2007, E05S05.

[7] A. Dessler, *Physics of the Jovian Magnetosphere*. Cambridge, U.K.: Cambridge Univ. Press, 2002.

[8] J.-M. Griessmeier, U. Motschmann, G. Mann, and H. Rucker, "The influence of stellar wind conditions on the detectability of planetary radio emissions," *Astron. Astrophys.*, vol. 437, no. 2, pp. 717–726, Jul. 2005.

[9] E. Bigg, "Influence of the satellite Io on Jupiter's decametric emission," *Nature*, vol. 203, pp. 1008–1010, 1964.

[10] J. Menietti, D. Gurnett, W. Kurth, and J. Groene, "Control of Jovian radio emission by Ganymede," *Geophys. Res. Lett.*, vol. 25, pp. 4281–4284, 1998.

[11] J. Menietti, D. Gurnett, and I. Christopher, "Control of Jovian radio emission by Callisto," *Geophys. Res. Lett.*, vol. 28, pp. 3047–3050, 2001.

[12] C. Higgins, J. Menietti, and I. Christopher, "Europa control of Jovian radio emission: A Galileo study," *Geophys. Res. Lett.*, vol. 33, 2006, L14110.

[13] D. A. Gurnett, W. S. Kurth, G. B. Hospodarsky, A. M. Persoon, P. Zarka, A. Lecacheux, S. J. Bolton, M. D. Desch, W. M. Farrell, M. L. Kaiser, H.-P. Ladreiter, H. O. Rucker, P. Galopeau, P. Louarn, D. T. Young, W. R. Pryor, and M. K. Dougherty, "Control of Jupiter's radio emission and aurorae by the solar wind," *Nature*, vol. 415, pp. 985–987, 2002.

[14] P. Zarka, B. Cecconi, and W. Kurth, "Jupiter's low-frequency radio spectrum from Cassini/Radio and Plasma Wave science (RPWS) absolute flux density measurements: Cassini flyby of Jupiter," *J. Geophys. Res.—Space*, vol. 109, no. A10, pp. A09S15.1–A09S15.18, 2004.

[15] P. Zarka, "The auroral radio emissions from planetary magnetospheres—What do we know, what don't we know, and what do we learn from them?" *Adv. Space Res.*, vol. 12, pp. 99–115, 1992.

[16] P. Zarka, B. Pedersen, A. Lecacheux, M. Kaiser, M. Desch, W. Farrell, and W. Kurth, "Radio emissions from Neptune," in *Neptune and Triton*. Tucson, AZ: Univ. Arizona Press, 1995, pp. 341–387.

[17] M. Kivelson, K. Khurana, C. Russell, R. Walker, J. Warnecke, F. Coroniti, C. Polanskey, D. Southwood, and C. Schubert, "Discovery of Ganymede's magnetic field by the Galileo spacecraft," *Nature*, vol. 384, pp. 537–541, Dec. 1996.

[18] E. Shoemaker, B. Lucchitta, J. Plescia, S. Squyres, and D. Wilhelms, "The geology of Ganymede," in *Satellites of Jupiter*. Tucson, AZ: Univ. Arizona Press, 1982, pp. 435–520.

[19] W. McKinnon and E. Parmentier, "Ganymede and Callisto," in *Satellites of Jupiter*. Tucson, AZ: Univ. Arizona Press, 1982, pp. 718–763.

[20] R. Pappalardo, G. Collins, J. Head, III, P. Helfenstein, T. McCord, J. Moore, L. Procktor, P. Schenk, and J. Spencer, "Geology of Ganymede," in *Jupiter: The Planet, Satellites and Magnetosphere*. Cambridge, U.K.: Cambridge Univ. Press, 2004, pp. 363–396.

[21] E. Parmentier, S. Squyres, J. Head, III, and M. Allison, "The tectonics of Ganymede," *Nature*, vol. 295, pp. 290–293, 1982.

[22] R. T. Pappalardo, J. W. Head, G. C. Collins, R. L. Kirk, G. Neukum, J. Oberst, B. Giese, R. Greeley, C. R. Chapman, P. Helfenstein, J. M. Moore, A. McEwen, B. R. Tufts, D. A. Senske, H. H. Breneman, and K. Klaasen, "Grooved terrain on Ganymede: First results from Galileo high-resolution imaging," *Icarus*, vol. 135, pp. 276–302, 1998.

[23] T. B. McCord, G. B. Hansen, R. N. Clark, P. D. Martin, C. A. Hibbitts, F. P. Fanale, J. C. Granahan, M. Segura, D. L. Matson, T. V. Johnson, R. W. Carlson, W. D. Smythe, and G. E. Danielson, The NIMS Team, "Non-water-ice constituents in the surface material of the icy Galilean satellites from the Galileo near-infrared mapping spectrometer investigation," *J. Geophys. Res.*, vol. 103, no. E4, pp. 8603–8626, 1998.

[24] J. Anderson, G. Schubert, R. Jacobson, E. Lau, W. Moore, and J. Palguta, "Discovery of mass anomalies on Ganymede," *Science*, vol. 305, pp. 989–991, 2004.

[25] J. Palguta, J. Anderson, G. Schubert, and W. Moore, "Mass anomalies on Ganymede," *Icarus*, vol. 180, pp. 428–441, 2006.

[26] M. Kivelson, K. Khurana, and M. Volwerk, "The permanent and inductive magnetic moments of Ganymede," *Icarus*, vol. 157, no. 2, pp. 507–522, 2002.

[27] O. Kuskov and V. Kronrod, "Internal structure of Europa and Callisto," *Icarus*, vol. 177, no. 2, pp. 550–569, 2005.

[28] R. Greeley, J. Klemaszewski, and R. Wagner, "Galileo views of the geology of Callisto," *Planetary Space Sci.*, vol. 48, no. 9, pp. 829–853, 2000.

[29] T. Spohn and G. Schubert, "Oceans in the icy Galilean satellites of Jupiter?" *Icarus*, vol. 161, no. 2, pp. 456–467, 2003.

[30] G. Johari and S. Jones, "The orientation polarization in hexagonal ice parallel and perpendicular to the c-axis," *J. Glaciol.*, vol. 21, pp. 259–276, 1978.

[31] T. Matsuoka, S. Fujita, S. Morishima, and S. Mae, "Precise measurement of dielectric anisotropy in ice Ih at 39 GHz," *J. Appl. Phys.*, vol. 81, no. 5, pp. 2344–2348, 1997.

[32] T. McCord, G. Hansen, and C. Hibbitts, "Hydrated salt minerals on Ganymede's surface: Evidence of an ocean below," *Science*, vol. 292, pp. 1523–1525, 2001.

[33] C. Chyba, S. Ostro, and B. Edwards, "Radar detectability of a subsurface ocean on Europa," *Icarus*, vol. 134, pp. 292–302, 1998.

[34] J. Moore, "Models of radar absorption in Europan ice," *Icarus*, vol. 147, pp. 292–300, 2000.

[35] A. Sihvola and J. Kong, "Effective permittivity of dielectric mixtures," *IEEE Trans. Geosci. Remote Sens.*, vol. GRS-26, no. 4, pp. 420–429, Jul. 1988.

[36] A. Sihvola and J. Kong, "Correction to 'effective permittivity of dielectric mixtures'," *IEEE Trans. Geosci. Remote Sens.*, vol. 27, no. 1, pp. 101–102, Jan. 1989.

[37] A. Ishimaru, *Wave Propagation and Scattering in Random Media*. New York: Academic, 1978.

[38] J. Eluszkiewicz, "Dim prospects for radar detection of Europa's ocean," *Icarus*, vol. 170, pp. 234–236, 2004.

[39] L. J. Porcello, R. L. Jordan, J. S. Zelenka, G. F. Adams, R. J. Phillips, W. E. Brown, Jr., S. H. Ward, and P. L. Jackson, "The Apollo lunar sounder radar system," *Proc. IEEE*, vol. 62, no. 6, pp. 769–783, Jun. 1974.

[40] G. Picardi, J. J. Plaut, D. Biccari, O. Bombaci, D. Calabrese, M. Cartacci, A. Cicchetti, S. M. Clifford, P. Edenhofer, W. M. Farrell, C. Federico, A. Frigeri, D. A. Gurnett, T. Hagfors, E. Heggy, A. Herique, R. L. Huff, A. B. Ivanov, W. T. K. Johnson, R. L. Jordan, D. L. Kirchner, W. Kofman, C. J. Leuschen, E. Nielsen, R. Orosei, E. Pettinelli, R. J. Phillips, D. Plettemeier, A. Safaenili, R. Seu, E. R. Stofan, G. Vannaroni, T. R. Watters, and E. Zampolini, "Radar soundings of the subsurface of Mars," *Science*, vol. 310, pp. 1925–1928, Dec. 2005.

[41] J. J. Plaut, G. Picardi, A. Safaenili, A. B. Ivanov, S. M. Milkovich, A. Cicchetti, W. Kofman, J. Mouginot, W. M. Farrell, R. J. Phillips, S. M. Clifford, A. Frigeri, R. Orosei, C. Federico, I. P. Williams, D. A. Gurnett, E. Nielsen, T. Hagfors, E. Heggy, E. R. Stofan, D. Plettemeier, T. R. Watters, C. J. Leuschen, and P. Edenhofer, "Subsurface radar sounding of the South Polar Layered Deposits of Mars," *Science*, vol. 316, pp. 92–95, 2007.

[42] R. Seu, R. J. Phillips, G. Alberti, D. Biccari, F. Bonaventura, M. Bortone, D. Calabrese, B. A. Campbell, M. Cartacci, L. M. Carter, C. Catallo, A. Croce, R. Croci, M. Cutigni, A. Di Placido, S. Dinardo, C. Federico, E. Flamini, F. Fois, A. Frigeri, O. Fuga, E. Giacomoni, Y. Gim, M. Guelfi, J. W. Holt, W. Kofman, C. J. Leuschen, L. Marinangeli, P. Marras, A. Masdea, S. Mattei, R. Mecozzi, S. M. Milkovich, A. Morlupi, J. Mouginot, R. Orosei, C. Papa, T. Paternò, P. Persi del Marmo, E. Pettinelli, G. Pica, G. Picardi, J. J. Plaut, M. Provenziani, N. E. Putzig, F. Russo, A. Safaenili, G. Salzillo, M. Rosaria Santovito, S. E. Smrekar, B. Tattarletti, and D. Vicari, "Accumulation and erosion of Mars' South Polar Layered Deposits," *Science*, vol. 317, pp. 1715–1718, Sep. 2007.

[43] J. Mouginot, W. Kofman, A. Safaenili, C. Grima, A. Herique, and J. Plaut, "MARSIS surface reflectivity of the South residual cap of Mars," *Icarus*, vol. 201, no. 2, pp. 454–459, 2009.

[44] M. Bland, A. Showman, and G. Tobie, "The orbital-thermal evolution and global expansion of Ganymede," *Icarus*, vol. 200, pp. 207–221, 2009.

[45] A. Showman, D. Stevenson, and R. Malhotra, "Coupled orbital and thermal evolution of Ganymede," *Icarus*, vol. 129, pp. 367–383, 1997.

[46] W. Kofman, R. Orosei, and E. Pettinelli, "Radar signal propagation and detection through ice," *Space Sci. Rev.*, vol. 153, pp. 249–271, 2010.

[47] S. Fujita, T. Matsuoka, T. Ishida, K. Matsuoka, and S. Mae, "A summary of the complex dielectric permittivity of ice in the megahertz range and its applications for radar sounding of polar ice sheets," in *Physics of Ice Core Records*. Sapporo, Japan: Hokkaido Univ. Press, 2000, pp. 185–212.

[48] H. Cane, "Spectra of the nonthermal radio radiation from the galactic polar regions," *Mon. Not. R. Astron. Soc.*, vol. 189, p. 465, 1979.

[49] R. Kirk, *Personal Communication*, 2000.

[50] J. Ogilvy, *Theory of Wave Scattering From Random Rough Surfaces*. London, U.K.: Taylor & Francis, 1991.

[51] G. Picardi, D. Biccari, A. Bazzoni, F. Fois, M. Iorio, R. Seu, P. Melacci, C. Federico, A. Frigeri, G. Minelli, L. Marinangeli, R. Orosei, D. Calabrese, E. Zampolini, W. T. K. Johnson, R. L. Jordan, J. Plaut, and A. Safaenili, "Mars Advanced Radar for Subsurface and Ionosphere Sounding (MARSIS): Subsurface performances evaluation," in *Proc. IEEE Radar Conf.*, Pasadena, CA, May 4–8, 2003, pp. 515–521.

[52] B. Giese, J. Oberst, T. Roatsch, G. Neukum, J. Head, III, and R. Pappalardo, "The local topography of Uruk Sulcus and Galileo Regio obtained from stereo images," *Icarus*, vol. 135, pp. 303–316, 1998.

[53] P. Schenk, W. McKinnon, D. Gwynn, and J. Moore, "Flooding of Ganymede's bright terrains by low-viscosity water-ice lavas," *Nature*, vol. 410, no. 6824, pp. 57–60, 2001.

[54] P. Schenk, "Slope characteristics of Europa: Constraints for landers and radar sounding," *Geophys. Res. Lett.*, vol. 36, 2009, L15204.

[55] R. Orosei, R. Bianchi, A. Coradini, S. Espinasse, C. Federico, A. Ferricioni, and A. Gavrishin, "Self-affine behavior of Martian topography at kilometer scale from Mars Orbiter Laser Altimeter data," *J. Geophys. Res.*, vol. 108, no. E4, p. 8023, 2003.

[56] G. Picardi, D. Biccari, R. Seu, J. Plaut, W. T. K. Johnson, R. L. Jordan, A. Safaenili, D. A. Gurnett, R. Huff, R. Orosei, O. Bombaci, D. Calabrese, and E. Zampolini, "MARSIS: Mars advanced radar for subsurface and ionosphere sounding," in *Mars Express: The Scientific Payload*, A. Wilson, Ed. Noordwijk, The Netherlands: ESA Publications Division, 2004, pp. 51–69, ISBN 92-9092-556-6.

[57] M. Skolnik, *Radar Handbook*, ser. Electronics electrical engineering. New York: McGraw-Hill, 2008.

[58] I. G. Cumming and F. H. Wong, *Digital Processing of Synthetic Aperture Radar Data: Algorithms and Implementation*. Reading, MA: Artech House, 2005.

[59] B. Mandelbrot, *The Fractal Geometry of Nature*. New York, U.S.: Freeman, 1983.

[60] G. Franceschetti, A. Iodice, M. Migliaccio, and D. Riccio, "Scattering from natural rough surfaces modeled by fractional Brownian motion two-dimensional processes," *IEEE Trans. Antennas Propag.*, vol. 47, no. 9, pp. 1405–1415, Sep. 1999.

[61] M. Shepard and B. Campbell, "Radar scattering from a self-affine fractal surface: Near-nadir regime," *Icarus*, vol. 141, pp. 156–171, 1999.

[62] G. Picardi, D. Biccari, R. Seu, L. Marinangeli, W. T. K. Johnson, R. L. Jordan, J. Plaut, A. Safaenili, D. A. Gurnett, G. G. Ori, R. Orosei, D. Calabrese, and E. Zampolini, "Performance and surface scattering models for the Mars Advanced Radar for Subsurface and Ionosphere Sounding (MARSIS)," *Planetary Space Sci.*, vol. 52, pp. 149–156, 2004.

[63] R. Seu, D. Biccari, R. Orosei, L. V. Lorenzoni, R. J. Phillips, L. Marinangeli, G. Picardi, A. Masdea, and E. Zampolini, "SHARAD: The MRO 2005 shallow radar," *Planetary Space Sci.*, vol. 52, pp. 157–166, 2004.

ABOUT THE AUTHORS

Lorenzo Bruzzone (Fellow, IEEE) received the Laurea (M.S.) degree in electronic engineering (*summa cum laude*) and the Ph.D. degree in telecommunications from the University of Genoa, Genoa, Italy, in 1993 and 1998, respectively.

Currently, he is a Full Professor of Telecommunications at the University of Trento, Trento, Italy, where he teaches remote sensing, pattern recognition, radar, and electrical communications. He is the Head of the Remote Sensing Laboratory in the Department of Information Engineering and Computer Science, University of Trento. His current research interests are in the areas of remote sensing, radar and synthetic aperture radar, signal processing, and pattern recognition. He conducts and supervises research on these topics within the frameworks of several international and national projects. He is the author (or coauthor) of 101 scientific publications in referred international journals (68 in IEEE journals), more than 150 papers in conference proceedings, and 15 book chapters. He is editor/coeditor of ten books/conference proceedings and one scientific book.

Dr. Bruzzone is a referee for many international journals and has served on the Scientific Committees of several international conferences. He is a member of the Managing Committee of the Italian Inter-University Consortium on Telecommunications and a member of the Scientific Committee of the India-Italy Center for Advanced Research. Since 2009, he has been a member of the Administrative Committee of the IEEE Geoscience and Remote Sensing Society. He ranked first place in the Student Prize Paper Competition of the 1998 IEEE International Geoscience and Remote Sensing Symposium (Seattle, WA, 1998). He was a recipient of the Recognition of the IEEE Transactions on Geoscience and Remote Sensing Best Reviewers in 1999 and was a Guest Coeditor of different Special Issues of the IEEE Transactions on Geoscience and Remote Sensing. In the past years joint papers presented by his students at international symposia and master theses that he supervised have received international and national awards. He was the General Chair and Co-Chair of the First and Second IEEE International Workshop on the Analysis of Multi-Temporal Remote-Sensing Images (MultiTemp), and is currently a member of the Permanent Steering Committee of this series of workshops. Since 2003, he has been the Chair of the SPIE Conference on Image and Signal Processing for Remote Sensing. From 2004 to 2006, he served as an Associated Editor of the IEEE Geoscience and Remote Sensing Letters, and currently is an Associate Editor for the IEEE Transactions on Geoscience and Remote Sensing and the *Canadian Journal of Remote Sensing*. Since April 2010, he has been the Editor of the IEEE Geoscience and Remote Sensing Newsletter. In 2008, he was appointed a member of the joint NASA/ESA Science Definition Team for the radar instruments for *Outer Planet Flagship Missions*. Since 2010, he has been in the Science Team of the Shallow Radar (SHARAD) onboard the NASA Mars Reconnaissance Orbiter. He is a member of the Italian Association for Remote Sensing (AIT).

Giovanni Alberti received the Degree (*cum laude*) in electronic engineering (telecommunication specialization) from the University "Federico II" of Naples, Naples, Italy, in 1989.

Currently, he works for the Consortium for the Research on Advanced Remote Sensing Systems. (CORISTA), Naples, Italy. His main research activities have dealt with the analysis and design of microwave sensors, such as synthetic aperture radar, radar altimeter, and ground penetrating radar, and image processing for use in the field of remote sensing. He is responsible of research projects sponsored by Italian and European Space Agency and NASA. In recent years, he was involved in both Mars (MARSIS and SHARAD) and Saturn (CASSINI) missions. He is member of Cassini Radar and SHARAD Science Teams, for which he is also the Italian Team Leader Deputy. He lectured on "Aerospace Remote Sensing Systems" at Seconda Università di Napoli.

Claudio Catallo received the Full Degree in electronic engineering from the University of Rome, Rome, Italy and the Italian Government full qualification in 1978.

Since 2006, he has coordinated around 200 operational and scientific activities to support the scientific communities, institutional customers, and experiment teams, for the GPRs Sounders embarked in Mars Express and Mars Reconnaissance Orbiter and Cassini radar in the TASI Observation System and Radar Business Line. From 1983 to 1990, he was responsible for three TLC S\Cs and Columbus ISS system verification activities. From 1980 to 1982, he was the Radar System Engineer in the former Contraves Italiana, from 1978 responsible in a restricted DOD staff during qualification and launch campaign for integrated radar defense system; in the previous years, he was a Test Engineer for the state of the art of audio measurements and author of more than 30 specialized magazine publications. He was an author and coauthor of papers that were presented at several conferences with main contributions to Mars (and Earth Analogues) subsurface probing, coordinating also the realization and launch of an SSR stratospheric mission, flown in 2009 over the North Pole. He is responsible for the TASI BL European Commission research programs. He is coordinator of NEWA and SIMTISYS European Commission (EC) programs and member of the LIMES and SEABILLA boards. From 1999 to 2002, he was the Head of the three engineering units in Telecommunication Directorate in the former Alenia Spazio, leading several international TLC programs and contributing to international workshops. From 1993 to 1999, he coordinated the design and realization of the electrical ground segment of the Globalstar Satellite Constellation and he was the Huyndai TAA Alenia Courses leader. From 1990 to 1993, he led two flight subsystem design and flight verifications of two Italian advanced TLC Satellites.

Dr. Catallo is International Union of Radio Science (URSI) and the American Institute of Aeronautics and Astronautics (AIAA) member since 1991.

Adamo Ferro (Student Member, IEEE) received the M.S. degree in telecommunications engineering (*summa cum laude*) from the University of Trento, Trento, Italy, in 2008, where he is currently working towards the Ph.D. degree in information and communication technologies.

During summer 2010, he was a visiting Ph.D. student at the Jet Propulsion Laboratory, California Institute of Technology/NASA, Pasadena. His main interests include the analysis of planetary radar sounder signals for information extraction purposes, and very high resolution synthetic aperture radar signal characterization in urban environments aimed at the automatic extraction of man-made structures. He is Participating Scientist of the SHAllow RADar (SHARAD) instrument science team.

Mr. Ferro was a recipient of the prize for the best Italian Master Thesis on Remote Sensing presented in 2008 awarded by the IEEE Geoscience and Remote Sensing South Italy Chapter.

Wlodek Kofman received the M.Sc degree in electronics from Warsaw Polytechnic, Warsaw, Poland, in 1968 and the Ph.D. degree in signal processing and Doctorat D'Etat in geophysics from University of Grenoble, Grenoble, France, in 1972 and 1979, respectively.

He is a Research Director at Centre National de la Recherche Scientifique and Science Advisor at research direction of l'Ecole Polytechnique, Paris, France. His main research activity is concerned with issues of signal processing, radar technique, plasma physics, study of earth high atmosphere and ionosphere, and planetaries surface and subsurface. He has given lectures at master and doctoral level in ionospheric physics, signal processing, and planetology. He is Principal Investigator of the CONSERT experiment on ESA cornerstone mission ROSETTA. He is Co-Investigator of sounder radars instruments on ESA, NASA, and JAXA space missions. He was Vice Chairman (1994–1997) and then Chairman (1997–1999) of international incoherent scatter radars facility EISCAT. He was Director of Laboratoire de Planetologie de Grenoble (1999–2007), and presently he is member of ESA Space Science Advisory Committee. He published more than 145 publications (including reports) and supervised 17 Ph.D. dissertations. *Asteroid* 13368 has been named «Wlodekofman» to honor Wlodek Kofman as "Principal Investigator on the Rosetta mission."

Dr. Kofman is an Honorary Fellow of the U.K. Royal Astronomical Society and a member of the American Geophysical Union (AGU). He was the Editor-in-Chief of *Annales Geophysicae* edited by The European Geosciences Union (2004–2010). He has been referee to various journals: *Journal of Atmospheric and Terrestrial Physics* (JASTP), *Journal of Geophysical Research* (JGR), *Radio Science*, *Geophysical Research Letters* (GRL), IEEE, *Annales Geophysicae*, *Signal Processing*.

Roberto Orosei received the B.S. (Laurea) degree in astronomy (*cum laude*) from the University of Bologna, Bologna, Italy, in 1992 and the Ph.D. degree in remote sensing from the Department of Engineering and Information Technology and Telecommunications, University of Rome "La Sapienza," Rome, Italy, in 1999.

He is currently Researcher at the Istituto di Fisica dello Spazio Interplanetario, Rome, Italy. He is Team Member of the Visual InfraRed Thermal Imaging Spectrometer (VIRTIS) experiment for ESA's Rosetta mission, Team Member of the SHAllow Radar (SHARAD) experiment for NASA's Mars Reconnaissance Orbiter mission, Team Member of the Visible and InfraRed (VIR) imaging spectrometer for NASA's Dawn mission, Team Member of the RADAR experiment for NASA's Cassini mission, Team Member of the Mars Multispectral Imager for Subsurface Studies (Ma_Miss) experiment for ESA's ExoMars mission, Team Member of the Jovian InfraRed Auroral Mapper (JIRAM) imaging spectrometer for NASA's Juno mission, and Deputy Principal Investigator of the Mars Subsurface and Ionosphere Radar Sounder (MARSIS) experiment for ESA's Mars Express mission. He has published more than 40 research papers in international scientific journals. His research topics include Mars geology, comet science, synthetic aperture radar data processing, numerical modeling of electromagnetic scattering and propagation, numerical modeling of diffusion processes, and numerical solution of partial differential equation.

Dr. Orosei was awarded a fellowship at the European Space Agency European Space Research and Technology Center (ESTEC) from 1994 to 1996. He is a reviewer for international scientific journals including *Planetary and Space Science*, *Advances in Space Research*, the IEEE TRANSACTIONS ON GEOSCIENCE AND REMOTE SENSING, and *Radio Science*.